Vegetation Canopy Reflectance Modeling through Turbid Medium Radiative Transfer

Barry D. Ganapol
Departments of Hydrology and Water Resources
and
Aerospace and Mechanical Engineering
University of Arizona
ganapol@cowboy.ame.arizona.edu

ABSTRACT

Biophysical considerations for vegetation canopy reflectance modeling are presented. Included is a brief overview outlining strengths and weaknesses of four possible canopy reflectance models. The overview is followed by the description of the **LCM2** coupled leaf/canopy turbid medium reflectance model based on natural averaging. The model follows conventional radiative transfer theory with modification for canopy architecture as characterized by leaf orientation. The presentation concludes with a demonstration of **LCM2** in a multiple pixel mode to estimate the amount of ripe coffee cherries at harvest in the fields of the Kauai Coffee Company and to detect targets hidden beneath canopies.

I. Introduction

Vegetation plays a significant role in sustaining life on planet Earth. In particular, vegetation is responsible for the exchange of O_2 and CO_2 to maintain an oxygen rich atmosphere and the conversion of the sun's energy into photosynthetic activity for nutrient biogeochemical recycling. In addition, the global climate is strongly linked to vegetation's existence and the ocean's activity. Thus humankind's very survival depends on the health of Earth's vegetation canopies. For this reason, as part of NASA's Earth Science Enterprise, a vegetation canopy research initiative has been active for the past 20 years. The goal of this effort has been to gain understanding of how radiant energy interacts with vegetation. Such understanding is essential if governments are to make sensible decisions concerning future development of Earth's resources while maintaining a commitment to the environment. In addition, a detailed knowledge of how these interactions lead to the canopy reflectance increases our understanding of nature's processes. For example, in the investigation of life sustaining photosynthesis and leaf evapo-transpiration, plant physiologists are primarily concerned with the complex biochemical interactions driven by radiant energy in the visible part of the sun's energy spectrum. The agronomist, on the other hand, is concerned with how the morphology of crop canopies influence leaf biochemistry to promote photosynthesis and subsequently yield. In these applications, the relative amounts of biochemical agents as well as the local environmental conditions and canopy architecture are primary factors in predicting canopy health and intra- and inter-annual photosynthetic gain. Fortunately, for both the plant physiologist and agronomist, information concerning biochemical agents in addition to canopy structural (photometric) characteristics can be inferred from the spectral variation of photons reflected from vegetation. The remote sensing of the reflected energy, therefore, can provide the opportunity to infer chemical content, canopy yield and

in general overall canopy health. This information is encoded in the canopy spectral response to passive sunlight in the form of the canopy reflectance or, more generally, in the bi-directional reflectance distribution function (BRDF). The key to decoding this information in the spectral response is fundamental consideration of how a canopy influences that response through microscopic interactions of photons within leaves to the distribution of radiant energy across leaf aggregates. This is where radiative transfer enters the analysis.

I.1 Primary Science Issue

The fundamental science issue to be addressed here is

> "Can reflected information be reliably interpreted through the vegetation canopy reflectance?"

The magnitude of the undertaking can be assessed from Fig. 1. Sunlight penetrates the atmosphere, a portion of which is then reflected from the foliage, re-enters the atmosphere and is detected by an airborne or satellite sensor. The reflected photons contain information about the elements supported by the canopy such as fruits, branches, stems and leaves, as well as information concerning the soil and atmosphere. In order to distill the specific chemical information concerning the foliage contained in a detected signal, the undesired physical distortions introduced by the soil, atmosphere and canopy architecture must be accounted for. In principle, distortions can be removed through modeling the canopy reflectance (CR) with radiative transfer. Thus, the role of a canopy reflectance model is to enable the interpretation of remotely sensed observations of a canopy by removing that part of the signal that distorts the desired information whether that be chemical content, species or target identification.

I.2 Social Implications of CR Models

The social implications of a reliable canopy reflectance model are many. For instance in basic science, the understanding of the plant photo-systems can unlock the secrets of photosynthesis. At a more comprehensive level, CR investigations can lead to the establishment of ecological principles which could, in turn, provide improved forest management strategies. In the area of precision agriculture and crop management, properly interpreting remotely sensed information can improve crop yield and production efficiency thus benefiting humankind. Another significant application of CR modeling is to Global Climate models (GCMs) where canopy reflectance becomes the terrestrial boundary condition. While presently not as important as cloud forcing at this time, a representative boundary condition will, in future, progressively become more important as GCMs mature. Finally, in the military arena, reliable optical foliage reflectance models along with synthetic aperture radar (SAR) are an important component of precision battlefield engagement (PBE). They can provide warfighter asset management and estimation of adversary asset strength and location by enabling the detection of relocatable targets under foliage. In addition, such models can be used to design camouflage, concealment and detection (CC&D) to protect and assets or counter CC&D systems to more efficiently find targets. Hopefully, in this way, collateral damage could be limited with the goal of reducing unnecessary human causalities and property loss.

I.3 General CR Modeling Considerations

In considering a CR model, one must acknowledge that the ultimate goal is to uncover signatures. To do so, the following five prominent vegetation signatures play a significant role:

+ Spectral λ:	Wavelength response of canopy reflectance and transmittance indicating specific absorptions
+ Spatial ($\vec{r}$):	Arrangement of scattering objects within the canopy
+ Temporal (t):	Intra- and inter- annual variability
+ Direction (Ω):	Anisotropy from the canopy surface roughness
+ Polarization (Q):	Polarized state of reflected photons.

Variation with respect to the wavelength of the response is the most important signature. Indeed, the CR investigations are sometimes called hyperspectral investigations for this reason. In the canopy, the photons will selectively be scattered and absorbed at particular wavelengths. For example, as shown in Fig. 2, at water bands where the absorption is particularly high (~1100, 1450, 1920 nm), the signal will indicate photon depletion. At 550 nm, which is called the green peak, the reflectance will have a local maximum since the blue and red wavelength photons are strongly absorbed by chlorophyll on either side. The wavelength spectrum considered in the optical regime extends from ultra violet UV (400 nm) to the mid infrared MIR (2500 nm). Spatial signatures come from objects which are larger than the incident wavelengths of light and reflect light macroscopically. Such objects include hidden targets. The temporal signature is a result of changes in the canopy whether of anthropogenic (human made) or biogenic (naturally occurring) origin. Remote sensing addressing temporal variation is called change detection. Directional effects are caused by the canopy surface roughness leading to an anisotropic non-Lambertian response. In addition, the "hot spot" resulting from viewing in the retro direction (in the direction of the sun) where minimal shadowing is observed is a directional effect. Finally, polarization can be a relatively strong signature which can effectively be used to detect hidden human made targets. This is a result of the leaf surface being a weak natural linear polarizer and the leaf's interior essentially a non polarizer.

Canopy response signatures through the canopy reflectance are influenced by many factors. Some of these are the

+ size, shape and distribution of objects within the canopy
+ biophysical parameters such as
    - Leaf Area Index (LAI = canopy optical depth)
    - leaf optical properties
    - the sun (zenith) angle
    - Leaf Angle Distribution (LAD)
    - fAPAR--fraction of absorbed phytosynthetically active radiation.

I.4 A Brief Description of Canopy Reflectance Models

The interaction of radiant energy with plant canopies can be broadly characterized by the following four approaches.

A. Empirical Models

Probably the most simple of all modeling strategies is the empirical model. At the same time empirical models are the most inflexible and lead to the least amount of information. In this strategy, a surface is fit to the reflectance data. The simplest of all surfaces is the Lambertian surface empirical model for which the canopy reflectance is represented by [1]

$$R_f = \frac{\cos(\theta_i)}{\pi} E_i$$

where E_i is the incident radiance and θ_i is the sun zenith angle. While no surface is ever truly a Lambertian surface, this idealized assumption is used quite often because of its simplicity. A more complex representation is given by Minnaert's model [2]

$$R_f = c \frac{\left[\cos(\theta_i)\cos(\theta_\mathrm{v})\right]^k}{\cos(\theta_i)} E_i$$

and the Walthall model [3]

$$R_f = a + b\theta_\mathrm{v}\theta_i \cos(\phi_\mathrm{v} - \phi_i) + c\theta_\mathrm{v}^2\theta_i^2 + d\left[\theta_\mathrm{v}^2 + \theta_i^2\right]$$

where a,b,c,d and k are adjustable parameters and the subscripts i and v indicate incident and view directions respectively. One of the major limitations of empirical models is the lack of physical meaning of the parameters and thus the inability to adjust them for different physical situations. A second limitation is their use in directions for which they were not intended.

B. First Principle Physical Models

In this class of models, the turbid medium assumption figures prominently. This assumption is made to essentially enable the use of a modified form of conventional participating media radiative transfer theory as represented in Fig. 3. Specifically, the canopy is assumed to interact with photons as a (green) gas would. At this level of application, the photons do not sense the canopy structure and interact with the individual atoms assumed to be points. This assumption is also commonly called the atomistic assumption for obvious reasons. Contained in this supposition are the continuous media and far field assumptions. The medium is also assumed to be microscopically homogeneous. The discrete nature of the scattering centers and shadowing is therefore not part of the model and represents a significant limitation. These assumptions best fit a dense canopy. Canopy architecture is introduced via the leaf angle distribution (LAD) which accounts for the distribution of leaf orientations. In what follows, the **LCM2** model will be featured as an example of a first principles turbid medium model. The reference to first principles comes from the intent of these models to be primarily physically based with a minimal of adjustable parameters. Turbid medium modeling in it

present form originated at the Estonian School of Actinimetry headed by J. Ross in the mid 70's.

C. Geometric-Optic (GO) Models

In this formulation, the canopy is treated as an assemblage of vegetation filled 3D objects as shown in Fig. 4. Radiative transfer theory is assumed within the assemblages and shadowing is assumed between assemblages. An advantage of the GO model is indeed the inclusion of shadowing. A disadvantage is that a particular canopy realization must be specified and the statistical nature of a scene is lost.

D. Computer Simulation Models The final model category presents the most faithful depiction of vegetation canopies. Here ray tracing as shown in Fig. 5 is used to render a scene. Particles are tracked as they interact with the canopy leaves and other elements and are tallied as they cross specified areas. As one can imagine such a procedure is quite computationally intensive making inversion for canopy properties virtually impossible. In this category, radiosity is a commonly applied method of simulation. Here, leaves are considered as diffusely scattering surfaces. Each leaf can "communicate" with every other leaf through view factors as shown in Fig. 6. Radiosity models are also computationally intensive. Figure 7 shows a rendering from the Botanical Plant Modeling System (BPMS) which is one of the most effective rendering models currently available.

II. Description of the LCM2 Coupled leaf/Canopy Radiative Transfer (RT) Model

II.1 General Turbid Medium Canopy Modeling Considerations/Modeling Approach

By any estimation, the vegetation canopy (Fig. 8) represents an extremely complex biosystem that would seem to defy any consistent mechanistic analysis. In general, a canopy consists of stems, branches, flowering or non-flowering buds and leaves. In most CR modeling efforts, leaves are considered to be the primary scattering and absorbing element. Leaves are classified as either broad-leaf as found in deciduous vegetation or needle-leaf as found in fir trees. The complexity of a canopy makes the radiative transfer characterization ill posed. For example, questions arise such a---How are the medium biophysical properties to be appropriately defined?--- or How can the radiative transfer equation be written in a fractal-like setting?--- or How can radiative transfer be expected to provide a measure of the radiance when the medium is so biologically diverse? In a word, we are essentially "ignorant" when it comes to defining the radiative transfer setting. The approach taken in the development of the **LCM2** model [4] is to acknowledge our ignorance and to rely heavily on natural averaging. So rather than get consumed in modeling the detailed canopy structure or the detailed scattering of photons, we consider biophysical interactions in an average sense since our ignorance allows for nothing more. In conjunction with this modeling approach. we do not seek answers to difficult questions either. We only address the most basic of issues such as the determination of canopy reflectance on a mixed pixel by pixel basis or what is fAPAR---not the determination of specific species within a canopy or the hundreds of biochemical agents within a canopy. Another element of this modeling approach is that we can determine the minimum amount of detail required for an adequate description. In other

words—what we can get away with. In this regard, we will construct the simplest of models and compare to experiments to determine adequacy or not. If not, then additional effort is put into the model detail.

II.2 The Nested RT Model

The radiative transfer modeling approach most often taken in treating such a complex system is to consider intra-leaf and inter-leaf models separately. In the following, each sub-model in **LCM2** will be individually described. The collective model will include three sub-models--- for the leaf, the canopy and the bridge between them through the leaf reflectance and transmittance.

A. Within Leaf Scattering: The LEAFMOD Module

Observing Fig. 9 it comes as no surprise that the leaf is a complex multibodied structure of wax layers, elongated palisade parenchyma cells situated on top of a chaotically configured spongy mesophyll of vacuoles. Each region within the leaf has a specific function. For example, the light harvesting elements, called grana, are contained in the palisade parenchyma and are the initiators of photosynthesis. The function of the spongy mesophyll is to serve as a back scattering medium to optimize the capture of photons in the parenchyma by reducing non productive leakage of photons through the abaxial (bottom) leaf surface. The air-epicuticular wax interfaces called the upper and lower epidermis are defined by the outer leaf adaxial (top) and abaxial extent. The epidermal layers are composed of multilayered membranes of pectin, cellulose, cutin and wax and as will be seen are responsible for leaf polarization.

A.1. The Leaf Scattering Phase Function

The defining feature of the leaf radiative transfer model is the scattering phase function. The scattering phase function used in the **LEAFMOD** [5] module is the simplest possible in keeping with our ignorance. Therefore, we assume isotropic scattering. This choice is justified on the basis that photon deflection results from the change of the index of refraction at cellular walls. Since leaf cells, to a first approximation, are nearly circular, photons coming from all directions would, on average, experience uniform deflection in angle averaged over a cell as depicted in Fig. 10.

A.2. Radiative Transfer (RT) Equation

In order to avoid the complicating detail of the leaf configuration, an atomistic approximation of the leaf interior is assumed. This enables the use of the 1D radiative transfer equation

$$\left[\Omega\frac{\partial}{\partial\tau}+1\right]I(\tau,\Omega;\Omega_0)=\frac{\omega}{4\pi}\int_{4\pi}d\Omega' I(\tau,\Omega';\Omega_0)$$
$$I(0,\Omega;\Omega_0)=\delta(\Omega-\Omega_0)$$
$$I\left(\Delta_L,\Omega(-\mu,\phi);\Omega_0\right)=0$$

valid at each wavelength. I is the within leaf angular radiance. The longitudinal direction is measured from the adaxial surface as shown in Fig. 11. A light beam or

diffuse light is assumed to illuminate the top or bottom surface of the leaf resulting in light transmission through the leaf and reflectance from the leaf. Again a 1D model is preferred since nothing can be said about the 3D nature of the leaf with any confidence. In the RT model, the basic physical parameters are the scattering and absorption coefficients (or profiles) Σ_s, Σ_a, which are wavelength λ dependent, and the leaf thickness d_L.

A3 Within Leaf Radiance

The solution of the one angle (inclination) form of the equations is accomplished using Siewert' s FN method [6]. The solution strategy is to form two singular integral equations coupling the boundary radiances. These equations are solved by expanding the outgoing existences in a spectral approximation involving Legendre polynomial basis functions and finding the unknown (blending) coefficients by collocation and matrix inversion. The desired reflectance and transmittance outputs are shown in Fig. 12. The above transport formulation presupposes knowledge of the scattering Σ_s and absorption Σ_a coefficients respectively at each wavelength. Unfortunately, this information is not available like in the case of neutrons. For this reason, an additional calibration procedure must be performed.

A.4 Calibration of the Leaf Scattering Coefficient

To describe the scattering coefficient one could postulate a model of leaf scattering and determine an estimate of this coefficient as is done elsewhere. Here however, we choose to calibrate the scattering coefficient using experimental leaf reflectance and transmittance data. The procedure begins with the LOPEX/Leaf Data Set [7]. This is a dataset containing experimental leaf reflectances and transmittances measurements for about 70 broad leaf species over the wavelengths 400 nm to 2500 nm. The measurements are specified as the average of five repetitive measurements per species. In addition, the leaf average thickness and chemical assays are given. From this extensive dataset, it will be possible to calibrate the scattering profile Σ_s. The procedure is as follows. Say one is interested in determining the reflectance from a broad leaf maple canopy whose average leaf thickness is known as well as the amounts of chlorophyll, protein, cellulose and lignin and moisture are specified to simulate a particular environmental condition. This is called the leaf of interest (LoI-See Fig. 13). Next, a reference maple leaf is identified in the LOPEX library. The reference leaf (RF) will, of course, have a different thickness and chemical makeup relative to the LoI to be investigated; however, there will be several similarities. First, the primary biochemical agents will most likely be the same; and second, the scattering coefficients will be similar. The latter similarity is argued on the basis of how scattering comes about. Since scattering is a result of the variation of index of refraction across cell walls, the similarity of the leaf's anatomical structure over species would logically make the scattering coefficients similar. For this reason, the scattering within the RF is assumed to be the same as the LoI. Thus, the RF is used to determine (calibrate) the scattering coefficient of the LoI. This is accomplished by equating the experimental reflectance and transmittance measurements of LOPEX and the analytical expressions from the FN solution:

$$\rho_L\left(\Sigma'_a,\Sigma_s,d'_L;\lambda\right)=\rho_{EXP}$$
$$\tau_L\left(\Sigma'_a,\Sigma_s,d'_L;\lambda\right)=\tau_{EXP} \tag{1}$$

where

$$\rho_L\left(\Sigma'_a,\Sigma_s,d'_L\right)=\frac{\omega}{2}\sum_{\alpha=0}^{L-1}c_\alpha\int_0^1 d\mu\mu\phi_\alpha\left(-\mu\right) \tag{2a}$$

$$\tau_L\left(\Sigma'_a,\Sigma_s,d'_L\right)=\frac{\omega}{2}\sum_{\alpha=0}^{L-1}c_\alpha\int_0^1 d\mu\mu\phi_\alpha\left(\mu\right). \tag{2b}$$

The solution (inversion) to this set of nonlinear equations gives the absorption and scattering profiles for the RF:

$$\Sigma'_a(\lambda),\Sigma_s(\lambda) \tag{3}$$

The scattering coefficient is then assumed for the LoI, but the absorption coefficient is discarded since it is appropriate only for the RF. The absorption profile is reconstructed from the specific absorptivities σ_j associated with each major biochemical component:

$$\Sigma_a\equiv\sum_{j=1}^{J}\rho_j\sigma_j \tag{4}$$

where ρ_j is the density of component *j*. The specific absorptivities are obtained from the literature [7]. The final step is to run **LEAFMOD** in the forward mode to determine the leaf reflectance $\rho_L\left(\Sigma_a,\Sigma_s,d_L\right)$ and transmittance $\tau_L\left(\Sigma_a,\Sigma_s,d_L\right)$ for the LoI.

As an example how the calibration applies, consider a nominal maple leaf (LoI) with

d_L = 1.34 mm
ρ_w = 0.723 gm/cm^3
ρ_{ch} = 38.8 μg/cm^2.A representative maple leaf from LOPEX (RF), whose experimental reflectance and transmittance profiles will be used in eq(1), has d_L = 0.9 mm. Now consider two cases of canopy stress. The first case considers a chlorotic maple leaf where the chlorophyll concentration has been reduced to half its nominal value

$$\rho_{ch} = 19.4\ \mu g/cm^2.$$

For the second case, we consider a water stressed maple where the moisture contents is reduced by half

$$\rho_w = 0.367\ gm/cm^3\ .$$

Fig. 14 shows the resulting reflectances obtained from the calibration for both cases. Note that the chlorosis only effects the visible (400-680 nm) and the water stress only the NIR (700-2500 nm). Fig. 15 shows the variation over wavelength of the canopy reflectance for the two cases indicating the expected difference in reflectance from the nominal reflectance that should be observed. Thus, with this model, canopy reflectance can be leaf property specific which is the unique feature of **LCM2**.

B. The Leaf Area Scattering Phase Function: The Leaf/Canopy Connection

In this module, leaf optical properties are appropriately formulated for the canopy radiative transfer model. For this purpose, the leaf within the canopy is assumed to act as an idealized bi-Lambertian diffusely reflecting surface. Energy is assumed to be isotropically emitted from the leaf surfaces as shown in Fig. 16. The appropriate form for the leaf phase function is

$$\gamma_D(\Omega',\Omega;\Omega_L)=\begin{cases}\dfrac{1}{\pi}\rho_L|\Omega\cdot\Omega_L|, & (\Omega\cdot\Omega_L)(\Omega'\cdot\Omega_L)<0\\ \left(\dfrac{\pi}{2}-\theta\right) & \\ \dfrac{1}{\pi}\tau_L|\Omega\cdot\Omega_L|, & (\Omega\cdot\Omega_L)(\Omega'\cdot\Omega_L)>0.\end{cases} \tag{5}$$

The area scattering phase function is then defined as

$$\frac{1}{\pi}\Gamma_D(\Omega',\Omega)=\int_{2\pi} d\Omega_L|\Omega\bullet\Omega_L|g_L(\Omega_L)\gamma_D(\Omega',\Omega;\Omega_L) \tag{6}$$

where Ω',Ω are the incoming direction and outgoing directions respectively and $g_L(\Omega_L)$ is the leaf angle distribution (LAD). The LAD represents the leaf orientation within the canopy and is the characterizing feature of canopy architecture. The bi-Lambertian assumption, therefore, allows the LoI leaf reflectance and transmittance, ρ_L,τ_L as determined by **LEAFMOD**, to be used directly--- hence the connection between the LoI and the canopy. The one angle version or the diffuse area scattering phase function to be input into **CANMOD** is obtained by integration over the azimuthal angle

$$\Gamma_D(\mu',\mu)=2\int_{-1}^{1} d\omega g_L(\omega)a(\mu',\omega)b(\mu,\omega) \tag{7}$$

where the integrand is a relatively complicated function of both μ, μ' and μ_L.

The area scattering function also contains a term for specular reflection from the leaf surface as depicted in Fig. 17. The contribution can be expressed as

$$\Gamma_{sp}(\mu',\mu)=\frac{1}{4\pi}\int_0^{\pi} d\omega g_L\left(\mu_L^*[\cos(\omega)]\right)K\left(\kappa,\gamma[\cos(\omega)]\right)F_s\left(n,\gamma[\cos(\omega)]\right) \tag{8}$$

where the Fresnel coefficient is

$$F_s(n,\Omega' \bullet \Omega_L) = \frac{1}{2}\left[\frac{\sin^2(\gamma-\tilde{\gamma})}{\sin^2(\gamma+\tilde{\gamma})} + \frac{\tan^2(\gamma-\tilde{\gamma})}{\tan^2(\gamma+\tilde{\gamma})}\right] \qquad \tilde{\gamma} \equiv \sin^{-1}\left[\frac{\sin(\gamma)}{n}\right].$$

The specular component also introduces a linear polarizing component. There is experimental evidence [8] that leaves polarize the signal as a result of specular reflection from the leaf surface. The linear polarization component of the area scattering phase function is expressed as

$$\Gamma_Q(\mu',\mu) = \frac{1}{4\pi}\int_0^{\pi} d\omega g_L\left(\mu_L^*(\cos(\omega))\right) K\left(\kappa,\gamma\cos(\omega)\right) F_Q\left(n,\gamma\cos(\omega)\right) \qquad (9)$$

where

$$F_Q(n,\gamma) = \frac{1}{2}\left[\rho_{\parallel} - \rho_{\perp}\right]$$

and

$$r_{\parallel} = \frac{1}{2}\left[\frac{\sin^2(\gamma-\tilde{\gamma})}{\sin^2(\gamma+\tilde{\gamma})}\right]$$
$$r_{\perp} = \frac{1}{2}\left[\frac{\tan^2(\gamma-\tilde{\gamma})}{\tan^2(\gamma+\tilde{\gamma})}\right].$$

With polarization, the following area scattering phase matrix

$$\underline{\Gamma}(\mu',\mu) = \frac{1}{4\pi}\int_0^{\pi} d\omega g_L\left(\mu_L^*\right)\underline{L}\left(-\lambda\right)\bullet$$
$$\bullet K(\kappa,\gamma(\Omega'\bullet\Omega))\underline{T}(n,\gamma(\Omega'\bullet\Omega))\underline{L}\left(\lambda'\right) \qquad (10)$$

where

$$\underline{T}\left(n,\gamma\right) = \begin{bmatrix} F_s\left(n,\gamma\right) & F_Q\left(n,\gamma\right) \\ F_Q\left(n,\gamma\right) & F_s\left(n,\gamma\right) \end{bmatrix}$$

and

$$F_s(n,\gamma) = \frac{1}{2}[r_{\parallel} + r_{\perp}]$$
$$F_Q(n,\gamma) = \frac{1}{2}[r_{\parallel} - r_{\perp}].$$

The area scattering phase matrix $\underline{\Gamma}(\mu',\mu)$ is the "bridge" between leaf scattering and the canopy phase function as demonstrated in the following section.

C. Within Canopy Scattering: The CANMOD Module

C.1. The Canopy Radiative Transfer Algorithm

With the various scattering components now defined, a vector transport equation can be identified for the photon intensity and linear polarization components of the radiance. Only the simplest of polarization models (linear) will be considered since there is little information regarding circular or partial elliptical polarization states. With a transport equation set, the numerical solution methodology will then be described. Here we veer from the tried and true semi-analytical methods of **LCM2** used in the past to the standard discrete ordinates scheme however still with an emphasis on accuracy. Surprisingly, as will be shown, a very accurate method is developed by mining the solution through several convergence accelerators.

C.2 The Vector Transport Equation

Since we will only be concerned with the intensity and linear vertical polarization components, the appropriate transport equation will be for a 2-vector and not the usual 4-vector equation of elliptical polarization. The simplified Stokes vector is now defined as

$$\vec{I}(\tau,\mu) \equiv \begin{bmatrix} I(\tau,\mu) \\ Q(\tau,\mu) \end{bmatrix}. \tag{11}$$

The first component is the intensity which contains no information about the state of polarization unlike the second component which contains information concerning the linearly polarized state. The vector canopy transport equation that characterizes the variation of the Stokes vector as photons are scattered and absorbed in a vegetative medium can be written generally as

$$\left[\mu \underline{I}\frac{\partial}{\partial \tau} + G(\mu)\underline{I}\right]\vec{I}(\tau,\mu) = \int_{-1}^{1} d\mu' \underline{\Gamma}(\mu',\mu)\vec{I}(\tau,\mu') \tag{12}$$

The second term represents a total loss of photons in a beam of direction Ω necessitating that a photon be lost either by a scattering or an absorbing event. The intercept function G is given by

$$G(\Omega) = \frac{1}{2\pi}\int_{2\pi+} d\Omega_L |\Omega \bullet \Omega_L| g_L(\Omega_L) \tag{13}$$

and represents all the leaf area presented perpendicular to direction Ω. The boundary conditions at the upper canopy boundary ($\tau = 0$) and the lower boundary ($\tau = \Delta$) are

$$\begin{aligned} \vec{I}(0,\mu) &= \begin{bmatrix} 1 \\ 0 \end{bmatrix} \delta(\mu - \mu_0) \\ \vec{I}(\Delta,-\mu) &= 2\rho_T \int_0^1 d\mu' \mu' I(\Delta,\mu') \begin{bmatrix} 1 \\ p_T \end{bmatrix}. \end{aligned} \tag{14}$$

Unpolarized sunlight enters the canopy, is scattered and absorbed with a fraction linearly polarized and both unpolarized and polarized components can then be scattered back into the canopy by a partially Lambertian reflecting (target or soil) surface situated underneath the canopy. The strength of the reflected polarized signal from the surface is determined by an assigned degree of polarization p_T.

The solution is more conveniently obtained if the Stokes vector is decomposed into its uncollided and collided components

$$\vec{I}(\tau,\mu) = \vec{I}_0(\tau,\mu) + \vec{I}_c(\tau,\mu)$$

giving two transport equations

$$\left[\mu \underline{I} \frac{\partial}{\partial \tau} + G(\mu) \underline{I} \right] \vec{I}_0(\tau,\mu) = 0 \tag{15a}$$

$$\left[\mu \underline{I} \frac{\partial}{\partial \tau} + G(\mu) \underline{I} \right] \vec{I}_c(\tau,\mu) = \int_{-1}^{1} d\mu' \underline{\Gamma}(\mu',\mu) \vec{I}(\tau,\mu'). \tag{15b}$$

The uncollided contribution is easily solved

$$\vec{I}_0(\tau,\mu) = \begin{bmatrix} 1 \\ 0 \end{bmatrix} e^{-\tau/\xi} \delta(\mu - \mu_0) \Theta(\tau/\xi) \tag{16}$$

where $\xi \equiv \mu / G(\mu)$. Substituting the total vector into the second transport equation for the collided component gives

$$\left[\mu \underline{I}\frac{\partial}{\partial\tau}+G(\mu)\,\underline{I}\right]\vec{I}_c(\tau,\mu)=$$
$$=\int_{-1}^{1} d\mu'\underline{\Gamma}(\mu',\mu)\vec{I}_c(\tau,\mu')+\underline{\Gamma}(\mu_0,\mu)\begin{bmatrix}1\\0\end{bmatrix}e^{-\tau/\xi_\circ}$$
$$\vec{I}_c(0,\mu)=0 \qquad (17)$$
$$\vec{I}_c(\Delta,-\mu)=2\rho_T\left[\mu_0 e^{-\tau/\xi_\circ}+\int_0^1 d\mu'\mu' I_c(\Delta,\mu')\right]\begin{bmatrix}1\\p_T\end{bmatrix}$$

Once eq(17) is solved numerically for the angular intensity, the desired quantities are the vector reflectance

$$\vec{\rho}\equiv\begin{bmatrix}R_{fI}\\R_{fQ}\end{bmatrix}=\frac{1}{\mu_0}\int_0^1 d\mu'\mu'\vec{I}(0,-\mu') \qquad (18a)$$

as well as the degree of polarization at the top of canopy (ToC)

$$Dp_0\equiv\int_0^1 d\mu'\mu' Q(0,-\mu')/\int_0^1 d\mu'\mu' I(0,-\mu'). \qquad (18b)$$

C.3 The Converged SN (CSN) Algorithm

Simplicity and versatility are the hallmarks of the discrete ordinates (**SN**) numerical algorithm developed for neutron transport calculations but widely applied in all particle transport fields. The method amounts to a convenient bookkeeping scheme for a particle population as one sweeps in a specified direction across the spatial domain. Of course, inherent in the method are numerical errors resulting from the discretization of the spatial and angular domains; and as a result, the **SN** method has always been considered an approximate numerical scheme. In this section, a variation of the **SN** algorithm will be devised for radiative transfer in canopies. The methodology couples a Romberg iterative strategy with a Wynn-Epsilon (Wε) acceleration to generate nearly 4-place accuracy for the canopy reflectance.

C.3.1 SN/Romberg /Wε Theory

The method will be developed for the radiative transfer equation eq(15) for a slab of optical depth (LAI) Δ and an impinging (plane) beam source in direction μ_0 at ToC. At the bottom canopy boundary, a partially reflecting condition is imposed possibly representing a target or soil. After inclusion of the impinging source as a volume source, introducing the **SN** approximation and integrating over a spatial interval *h*, as shown in Fig. 18, we arrive at the **SN** equations without spatial approximation for the collided intensity $\vec{I}_c$

$$\mu_m\left[\vec{I}_{c,j+1,m}-\vec{I}_{c,j,m}\right]+G_m\int_h d\tau\vec{I}_{c,m}(\tau)=\sum_{m'=1}^{N}\omega_{m'}\underline{\Gamma}(\mu_{m'},\mu_m)\int_h d\tau\vec{I}_{c,m'}(\tau)+$$
$$+\xi_0\left[e^{-\tau_j/\xi_0}-e^{-\tau_{j+1}/\xi_0}\right]\underline{\Gamma}_{0,m}\begin{bmatrix}1\\0\end{bmatrix}, \tag{19a}$$

where

$$\vec{I}(\tau,\mu)=\vec{I}_0(\tau,\mu)+\vec{I}_c(\tau,\mu). \tag{19b}$$

and

$$\Gamma(\mu'_{m'},\mu_m)=\sum_{j=1}^{Lmc}\omega_j g_j a_{j,m} b_{j,m'}.$$

The *m*-subscript represents the angular discretization, while the *j*-subscript represents the spatial discretization at the interval edges. The angular quadrature points are chosen to be the zeros of the Legendre polynomial of degree *N/2* over the half ranges [-1,0] and [0,1]

$$P_{N/2}(\pm\mu_m)=0,\quad m=1,N/2.$$

The quadrature weights ω_m are for the corresponding Gauss/Legendre quadrature. Spatial discretization is uniform over [0,Δ] with

$$h\equiv\ \Delta/N_h.$$

In eq(19a), the following quantities have been defined:

$$\vec{I}_{c,j,m}\equiv\vec{I}_c(\tau_j,\mu_m)$$
$$G_m\equiv G(\mu_m)$$
$$\underline{\Gamma}_{m',m}\equiv\underline{\Gamma}(\mu_{m'},\mu_m).$$

If we were to follow the common practice of relating the integral of the intensity over interval *h* to the edge fluxes, we would call the average intensity (represented by the integrals) the average of the interval edge fluxes. Here, we adopt a more general view where the integration is interpreted as a quadrature approximation of a given order *K*

$$\int_h dx g(x)=\sum_{k=1}^{K}\alpha_k g_k+O(h^{K+1})$$

If a trapezoidal rule is assumed, then K is 3 and the α's are ½ and we have the usual "diamond difference" approximation. More importantly, we know the order of the error ($K = 2$) and the form of the error tail of the solution [9]

$$\vec{I}^{\,Exact}_{c,j,m} = \vec{I}_{c,j,m} + \sum_{k=1}^{\infty} \vec{\beta}_k h^{2k}. \tag{20}$$

With this knowledge, a Romberg iterative scheme [10] can be applied to eqs(19) in the fully discretized form

$$\begin{aligned} &\underline{T}^{-}_{m}\vec{I}_{c,j+1,m} - \underline{T}^{+}_{m}\vec{I}_{c,j,m} = \vec{q}_{j,m} + \\ &+\frac{h}{2}\sum_{m'=1,\neq m}^{N/2} \omega_{m'}\underline{\Gamma}_{m',m}\begin{bmatrix}\vec{I}_{c,j+1,m'} + \\ + \vec{I}_{c,j,m'}\end{bmatrix} + \\ &+\frac{h}{2}\sum_{m'=N/2+1,\neq m}^{N} \omega_{m'}\underline{\Gamma}_{m',m}\begin{bmatrix}\vec{I}_{c,j+1,m'} + \\ + \vec{I}_{c,j,m'}\end{bmatrix} \end{aligned} \tag{21}$$

with

$$\begin{aligned} \underline{T}^{-}_{m} &\equiv \left[\left(\mu_m + \frac{h}{2}G_m\right)\underline{I} - \omega_m\underline{\Gamma}_{m,m}\frac{h}{2}\right] \\ \underline{T}^{+}_{m} &\equiv \left[\left(\mu_m + \frac{h}{2}G_m\right)\underline{I} + \omega_m\underline{\Gamma}_{m,m}\frac{h}{2}\right] \\ \vec{q}_{j,m} &\equiv \xi_0\left[e^{-x_j/\xi_0} - e^{-x_{j+1}/\xi_0}\right]\underline{\Gamma}_{0,m}\begin{bmatrix}1\\0\end{bmatrix} \end{aligned}$$

in order to successively eliminate the higher order error terms in the error tail of eq(20). This is an extension of Richardson's extrapolation as applied previously to the transport equation.

C.3.2 Iteration Strategy

The SN algorithm of order N is implemented in the standard way with sweep iteration in the positive and negative angular directions. The convergence of the sweeps is accelerated using the Wynn-Epsilon algorithm. In this algorithm

$$\begin{aligned} &\varepsilon^{(n)}_{-1} = 0, \;\; \varepsilon^{(n)}_{0} = S_n \\ &\varepsilon^{(n)}_{k+1} = \varepsilon^{(n+1)}_{k} + \left[\varepsilon^{(n+1)}_{k} - \varepsilon^{(n)}_{k}\right]^{-1} \end{aligned}$$

S_n represents the sweep iterates and $\varepsilon_{2k}^{(n)}$ the subsequent improved approximation forming a tableau. The tableau diagonal is then interrogated for convergence of the canopy reflectance. Each S_n calculation contributes the first element of a Romberg scheme for convergence in spatial discretization. Finally, convergence in the quadrature order N is performed through a Wε acceleration.

III. LCM2 Demonstration

The three modules have been combined into the **LCM2** nested radiative transfer CR code. The code can be run in two distinct models---Single Pixel and Independent Pixel Approximations. In the section both modes will be demonstrated.

III.1 Single Pixel Approximation (SPA)

Figure 19 shows the variation of the reflectance of the intensity component for the visible and NIR wavebands for a canopy of with an LAI of 2 and erectophile (upright) LAD as the surface index of refraction varies. A constant soil background reflectance of 0.2 is assumed. The behavior is similar at all wavelengths. In particular, as the index of refraction increases from 1 (air) to 1.5, the reflectance increases. With increasing specular reflection from the leaf's adaxial surface, more photons avoid the leaf's interior and therefore there is less absorption and more can exit the canopy. This is in light of the tradeoff of less photons being diffusely scattered from the leaf's interior. The magnitude of the effect will no doubt depend on the canopy properties, but the tendency to increase reflection with increasing refractive index seems readily apparent.

Fig. 20 displays the change in the reflection of the Q-component with increasing index of refraction n. R_{fQ} also increases with n as does the degree of polarization at ToC. This is to be expected since an index of refraction different from 1 is the origin of linear polarization. It should also be noted that R_{fQ} does not exhibit the usual pronounced variation at the green peak associated with the leaf's interior. While there is some evidence of a green peak, there is no distinct chlorophyll well effect. This result is a direct consequence of the fact that polarization arises from the leaf surface as modeled. The slight rise at green (factor of 0.5 compared to a factor of 2 for R_f), is a result of multiple scattering of the intensity component providing the source of polarization. The difference between the two components is more clearly evident in Fig. 21 where the two components are shown for increasing canopy over-story (increasing canopy LAI). Saturation is observed in both components when, as the canopy become denser, there is little change in the reflectances. One difference to be noted is that with increasing LAI, R_f decreases in the visible and increases in the NIR. This is a result of the highly absorbing nature of the leaf in the visible--allowing increased absorption for a denser canopy and its highly scattering nature in the NIR--allowing increased probability of scattering out of the canopy. Also note that the increase in the NIR reflectance over the visible is a factor of two for the polarized component while it is a factor of 10 for the intensity component again a consequence of leaf surface scattering being responsible for polarization.

III.2 Independent Pixel Approximation (IPA)

A. Application to Precision Agriculture

Currently the transport development group at the University of Arizona is a part of a demonstration of the use of Un-piloted Aerial Vehicles (UAVs) by NASA in precision agriculture. In particular, the effort is focused on using a UAV to provide a synoptic view of the Kawai Coffee Company coffee fields. The Pathfinder UAV, carrying several cameras to record the visible and NIR reflectance shown in Fig. 22, was flown over the coffee fields. The intent of the campaign was to explore the possibility of transferring NASA technology to the agricultural community. **LCM2** in the IPA mode was the basis of a predictive Neural Net (NN) to distinguish the amount of yellow coffee cherries (the money crop) from green (under ripe) and red cherries (over ripe) in the fields. **LCM2** was used to train the NN to predict the three cherry classifications in a scene given reflectance estimates. The reflectances from the UAV flyover was then introduced as input and a prediction made based on the **LCM2** model as shown in Fig. 23. The prediction of yellow cherries agreed to within 10% of the ground truth which is rather remarkable agreement.

B. Linearly polarized Targets

Now consider a linearly polarizing target beneath the canopy. To test **LCM2** in a more realistic manner, a 64 (8x8) pixel scene was constructed. The LAI and soil reflectance were fixed at 2 and 0.2 for all pixels respectively and random amounts of 5 LAD distributions were assumed to represent a random LAD. Figure 25 shows the reflectances for the scene at three wavelengths 550 nm, 680 nm and 800 nm. For the same wavelengths, Fig. 26, shows a T-72 tank in the clear, which is subsequently to be hidden under a canopy of various LAIs. The vehicle surface is assumed to be fully linearly polarizing and reflects at 0.3. The surrounding soil is assumed to be reflecting at 0.1. Figures 27a,b show R_f and Dp0 for the T-72 under canopies of LAIs of 4 and 6. With increasing LAI, the T-72 becomes increasingly obscured in both measures as expected.

An alternative way of viewing the scene information is to plot the degree of polarization (Dp0) against R_f. When this is done for the canopy without a target we have Fig. 28a indicating no correlation between the degree of polarization and the R_f. Doing the same for the target under a canopy of LAI = 6 and recalling that the target could not be identified at all from the scene variations of R_f, and Dp0 individually, we observe the result that the T-72 target becomes clearly defined in all wavelengths with the NIR yielding the clearest definition. This result can be explained by noting that the T-72 is a much brighter object than the surrounding background and it polarizes while soil and canopy do not. In the Dp0/R_f plot this places the T-72 target in the upper right corner and the soil variation is confined to the bottom. The soil variation however still remains uncorrelated as in Fig. 28a on a very narrow scale. We believe this to be a very far significant result indeed.

Future Challenges of CR Modeling

Several serious challenges face canopy modelers in the future. One major challenge is the inverse problem of which the coffee cherry estimation is an example. Can canopy

parameters, important for ecological prediction, be obtained reliably? This challenge involves not only more powerful computational architectures, but also the development of fast running and accurate inversion algorithms. NNs are an example of the wave of new methods, but more powerful optimization concepts need to be developed if CR models are expected to see a routine use. Of course, this must go hand in hand with the development of larger memories and faster CPUs. The establishment of reliable canopy optical properties must also be part of the mix.

References

[1] B. Hapke and E. Wells, *J. Geophys Res*., **86**(B4), 3055-3060, (1981).
[2] M. Minnaert, *Astrophys. Jour*., **93**, 403-410 (1941).
[3] C. Walthal, et. al., *Appl. Opt*., **24**(3), 383-387 (1985).
[4] B. Ganapol ,et. al., *Rem. Sens. Environ.* **70**:153-166 (1999).
[5] B. Ganapol, et. al., *Rem. Sens. Environ.* **63**:182-193 (1998).
[6] C. Siewert, *Nucl. Sci. & Eng.*, **69**, 156-160 (1979).
[7] B. Hosgood, et. al. European Commission, Joint Research Centre, Institute for Remote Sensing Applications, Report EUR 16095 EN (1995).
[8] L. Grant, C. Daughtry., and V. Vanderbilt., *Envir. Exp. Bot*. **27**,139-145 (1987).
[9] E. Larsen and W.F. Miller, *Nucl. Sci.& Eng.*, **73**, 76-83 (1980).
[10] F. Press, *Numerical Recipes*, Cambridge Press, (2001).

Figures:

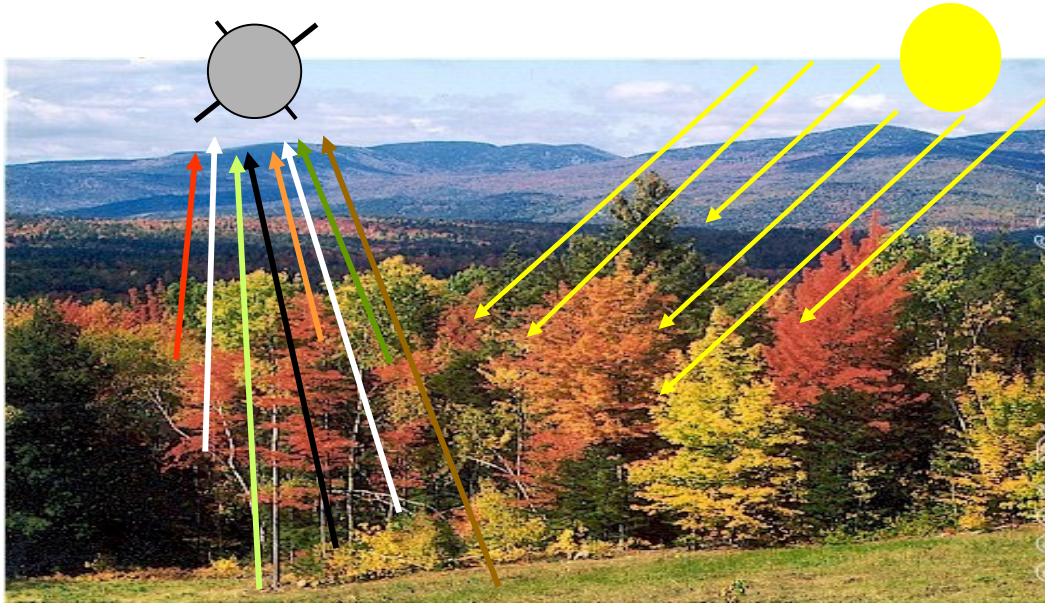

Fig. 1: Passive photons reflected from a canopy contain information about the canopy.

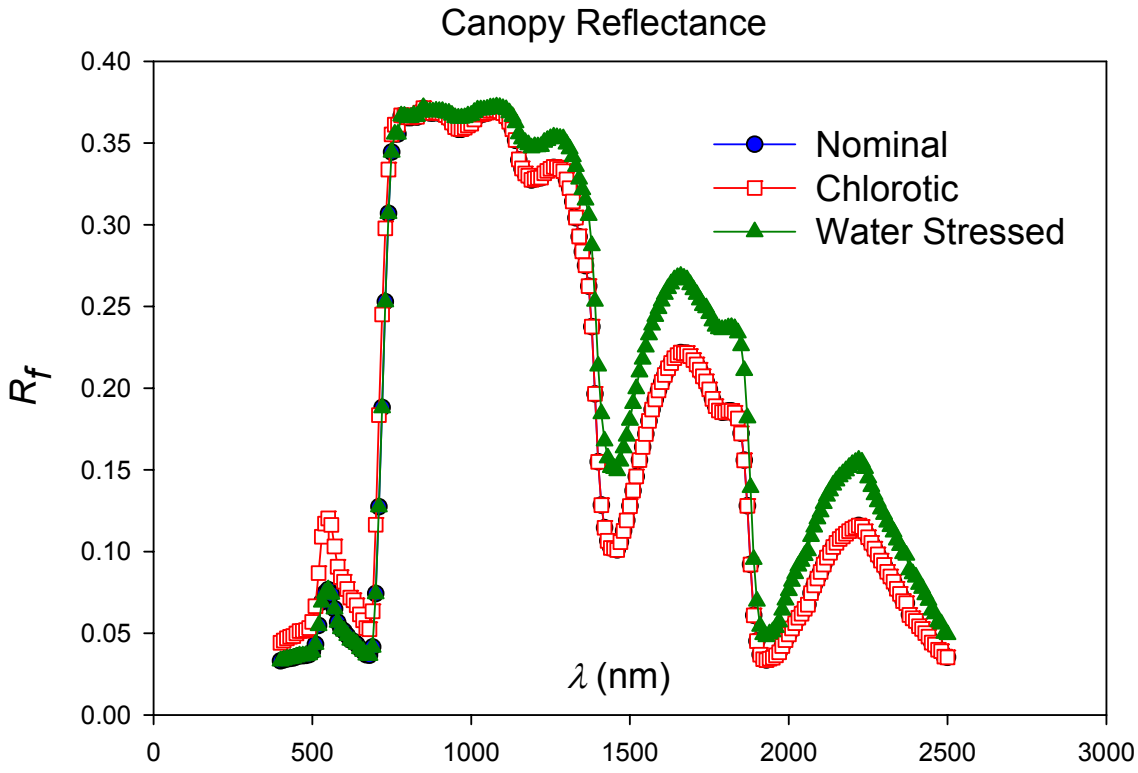

Fig. 2 A typical canopy reflectance spectrum.

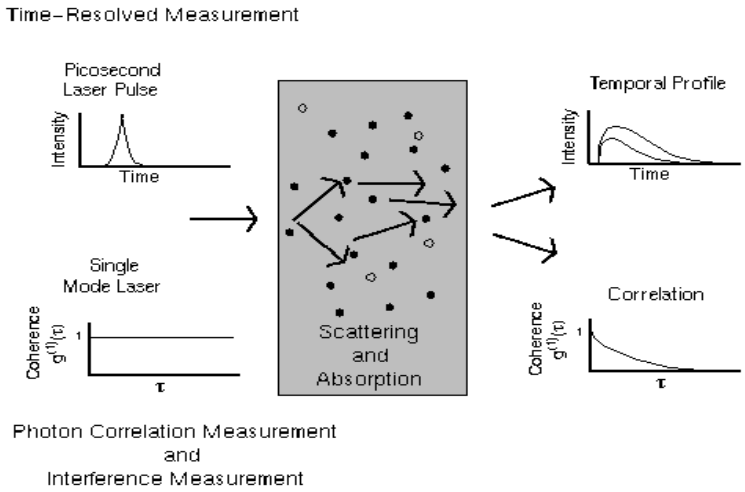

Fig. 3 Conventional radiative transfer participating medium.

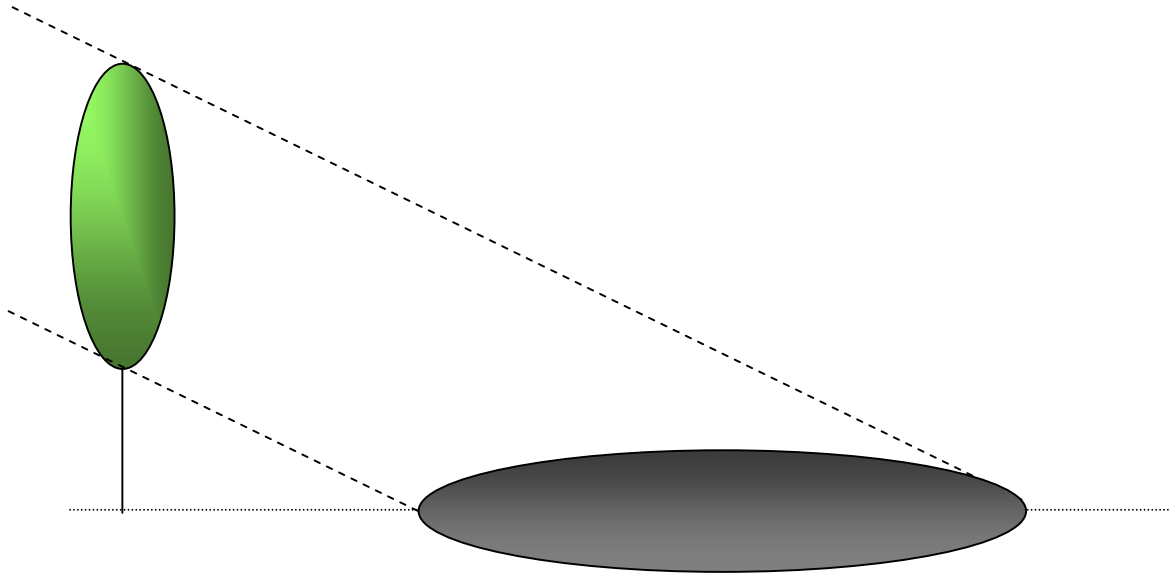

Fig. 4 Geometric-optic Model allows for shadows.

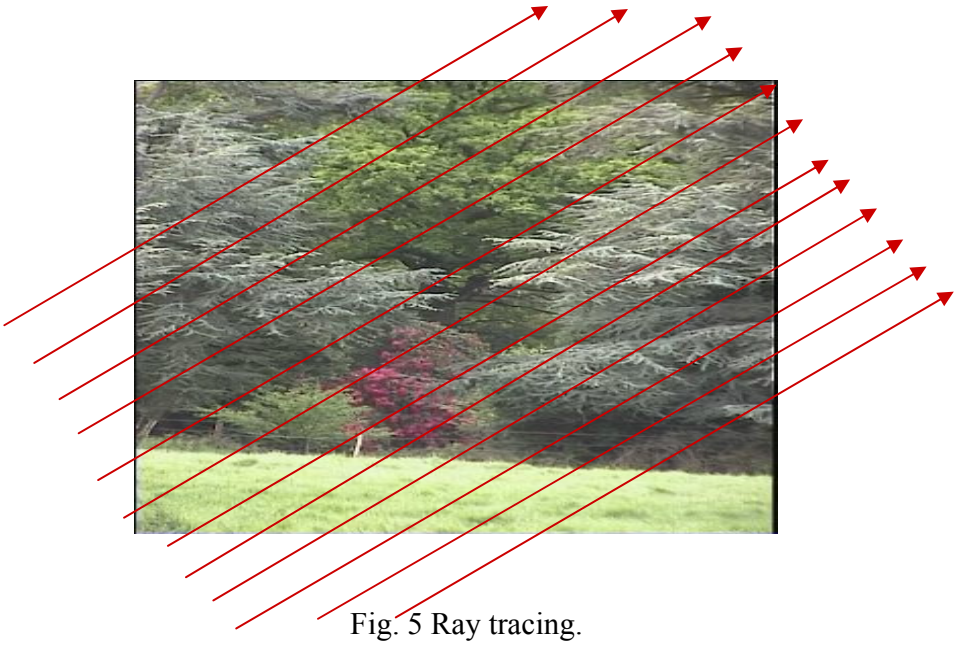

Fig. 5 Ray tracing.

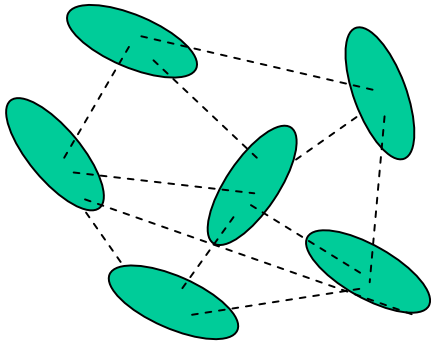

Fig. 6 Leaf communication in a radiosity models.

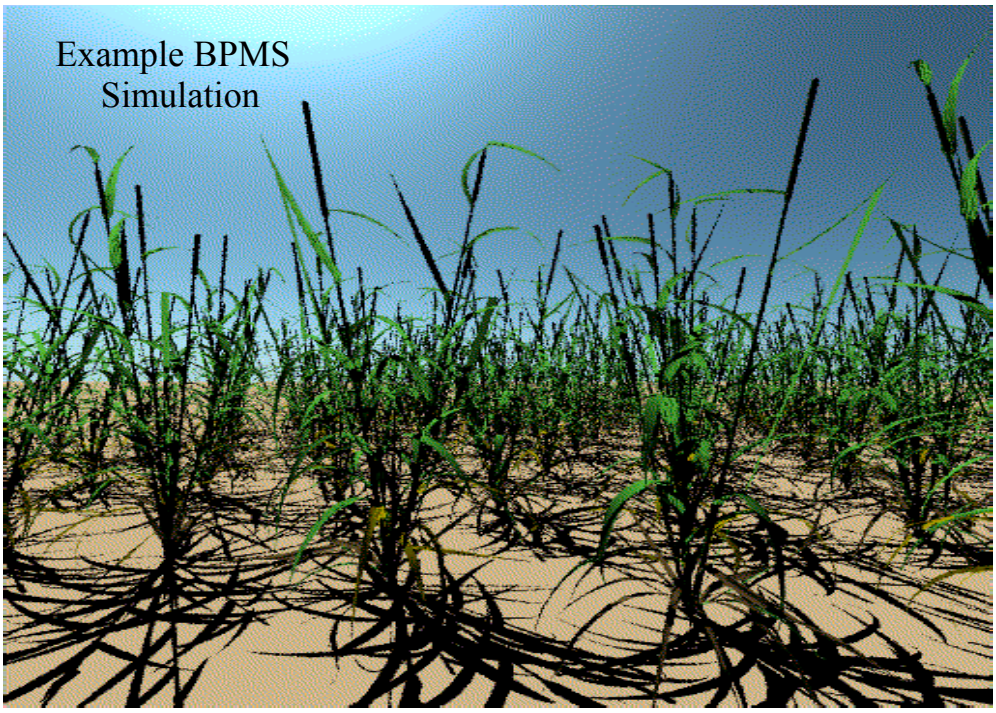

Fig. 7 Rendering from BPMS.

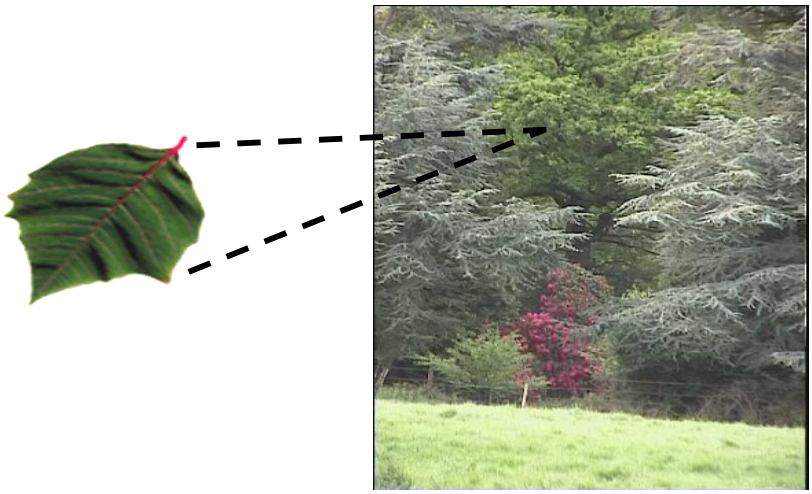

Fig. 8 A canopy is a very complicated biosystem.

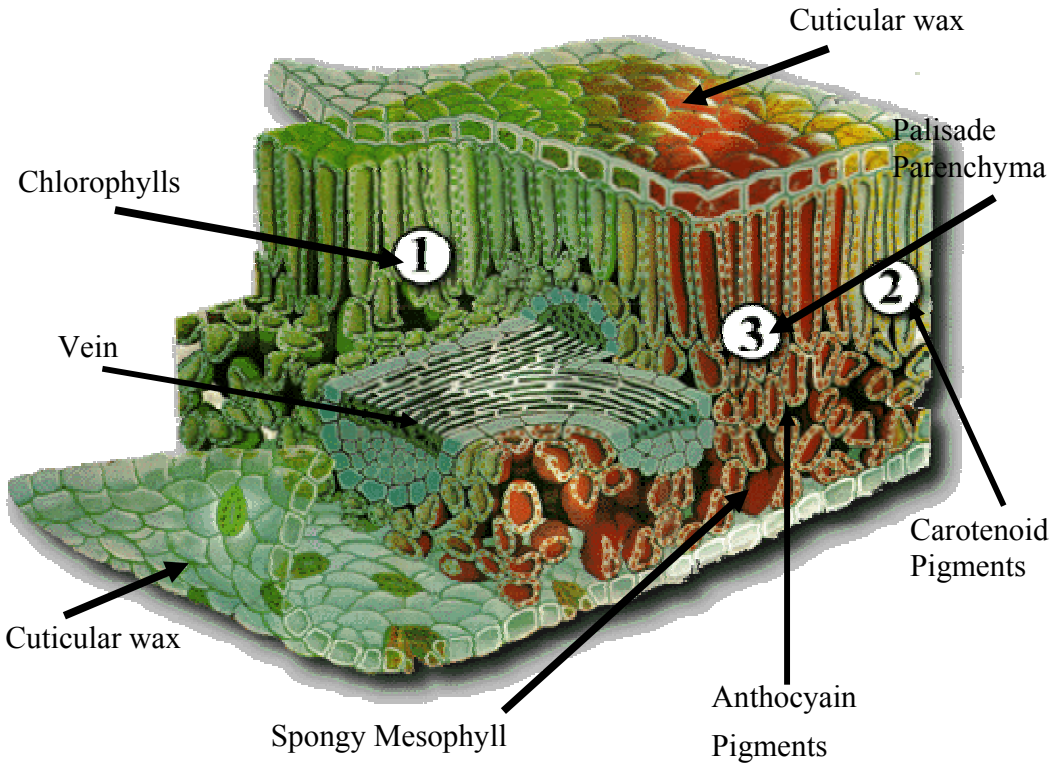

Fig. 9. Typical anatomical structure of a leaf.

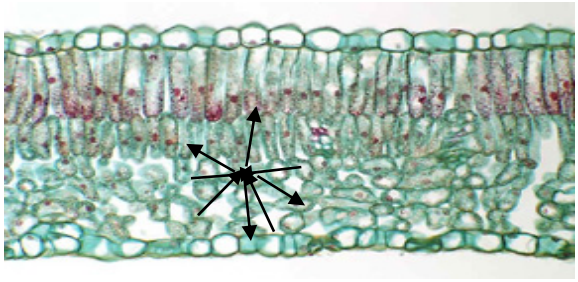

Fig.10 Isotropic within leaf scattering is assumed out of ignorance.

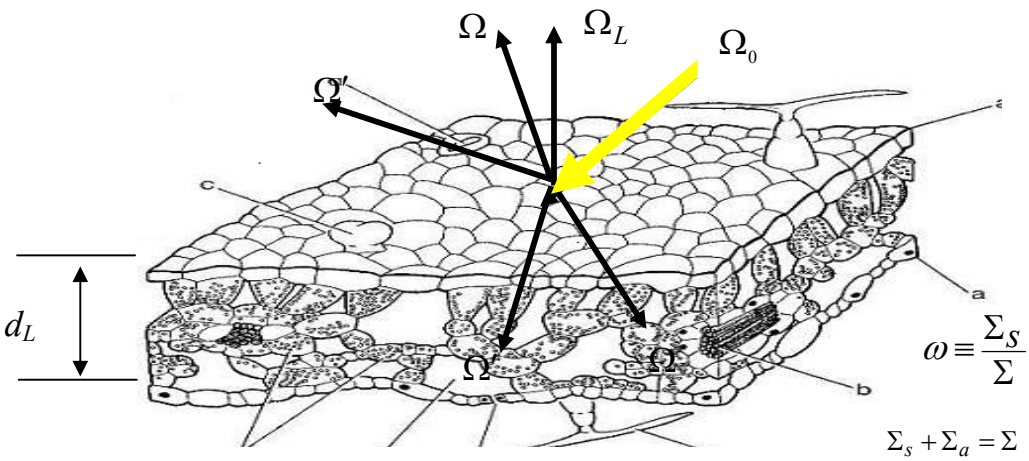

$$\Delta_L = d_L \Sigma$$

Fig. 11 Adaxial leaf surface illuminated by light beam or diffuse light.

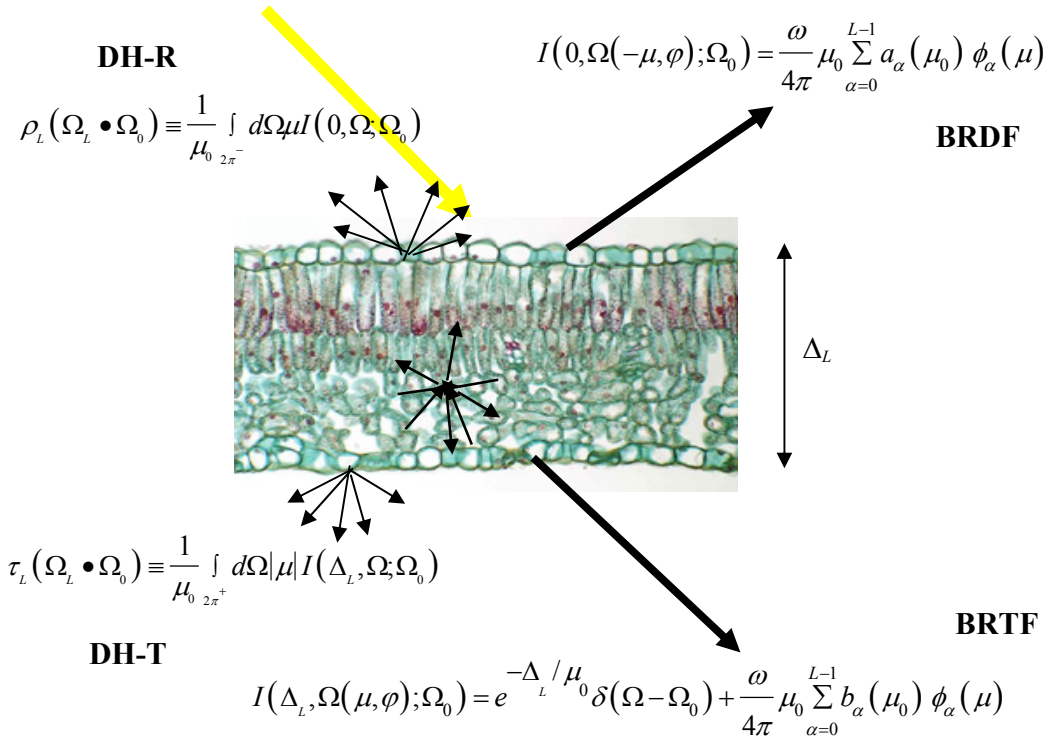

Fig. 12 Solution by the FN method.
(**D**=Direct/**H**=Hemispherical//**R**=reflectance/**T**=Transmittance))

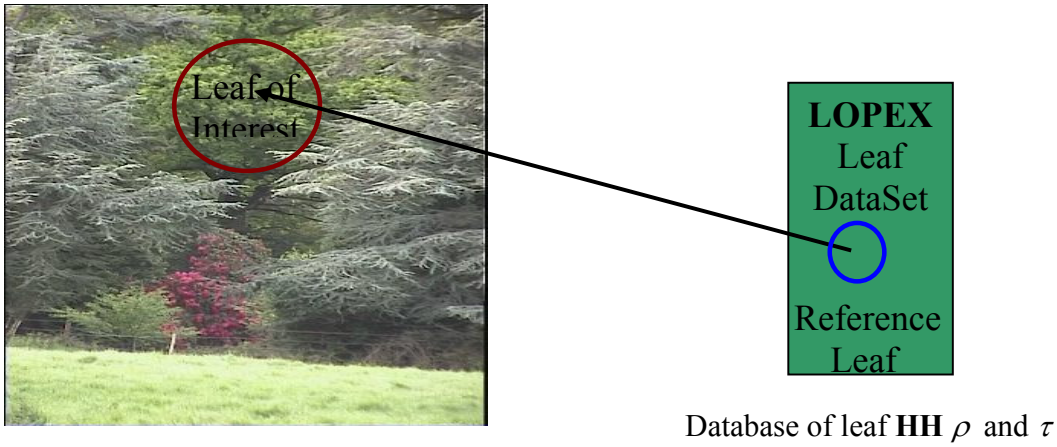

Fig. 13 Scattering within the reference leaf (RF) and leaf of interest (LoI) is similar.

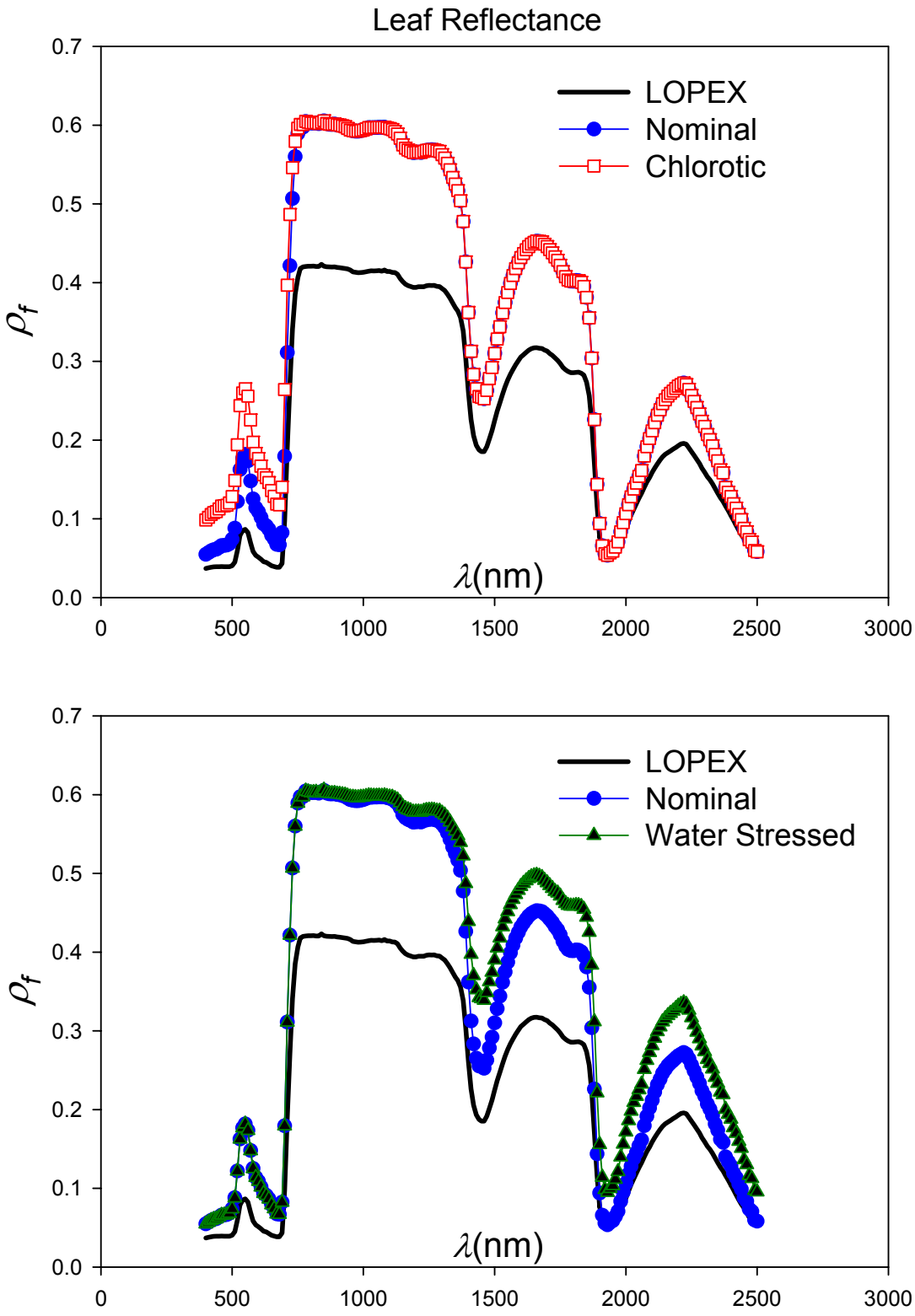

Fig. 14 Leaf reflectance for chlorotic and water stressed example.

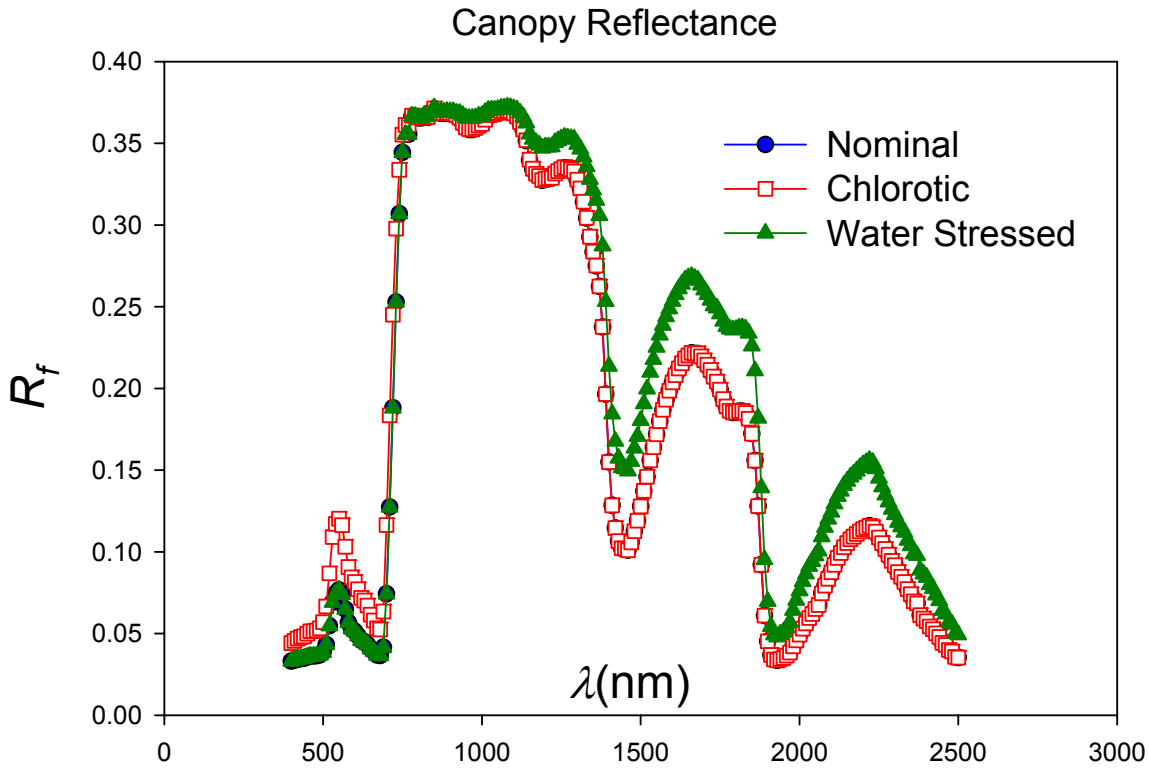

Fig. 15 Canopy reflectance for Chlorotic and water stressed canopies.

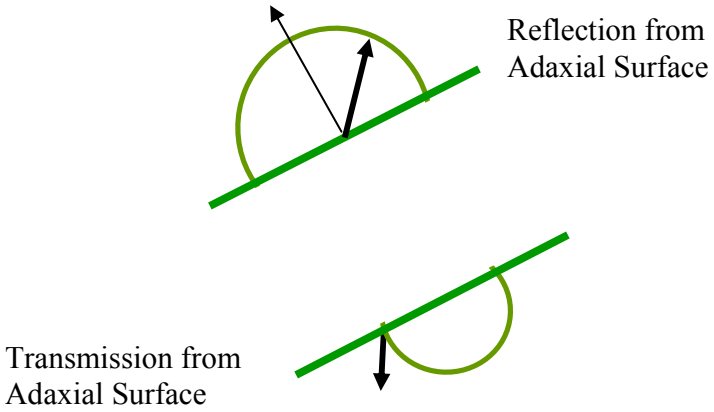

Fig. 16 Bi-Lambertian leaf scattering assumed within canopy.

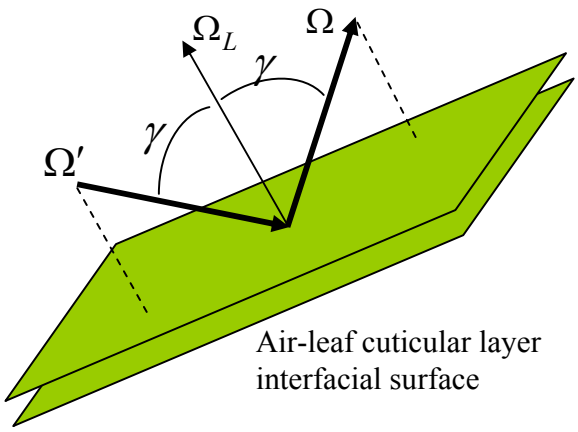

Fig. 17 Specular reflection at the leaf surface.

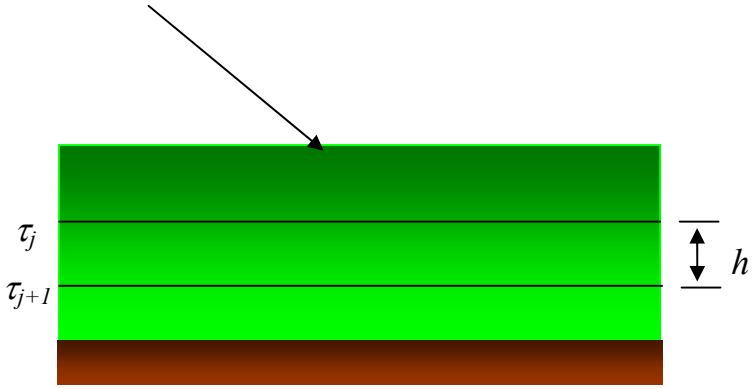

Fig. 18 Discretized spatial domain.

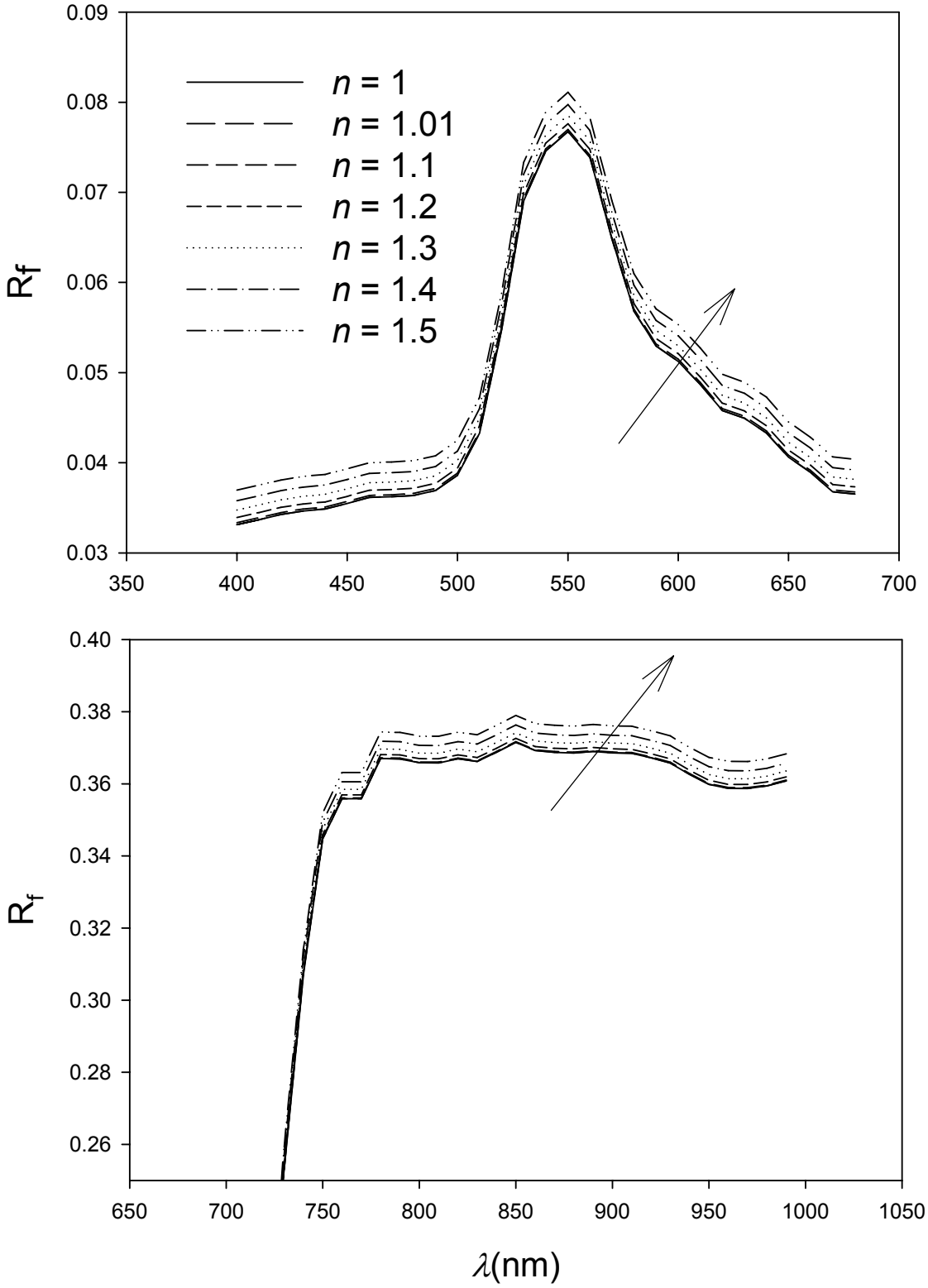

Fig. 19 Canopy reflectance with specular leaf reflection for an unpolarized target.

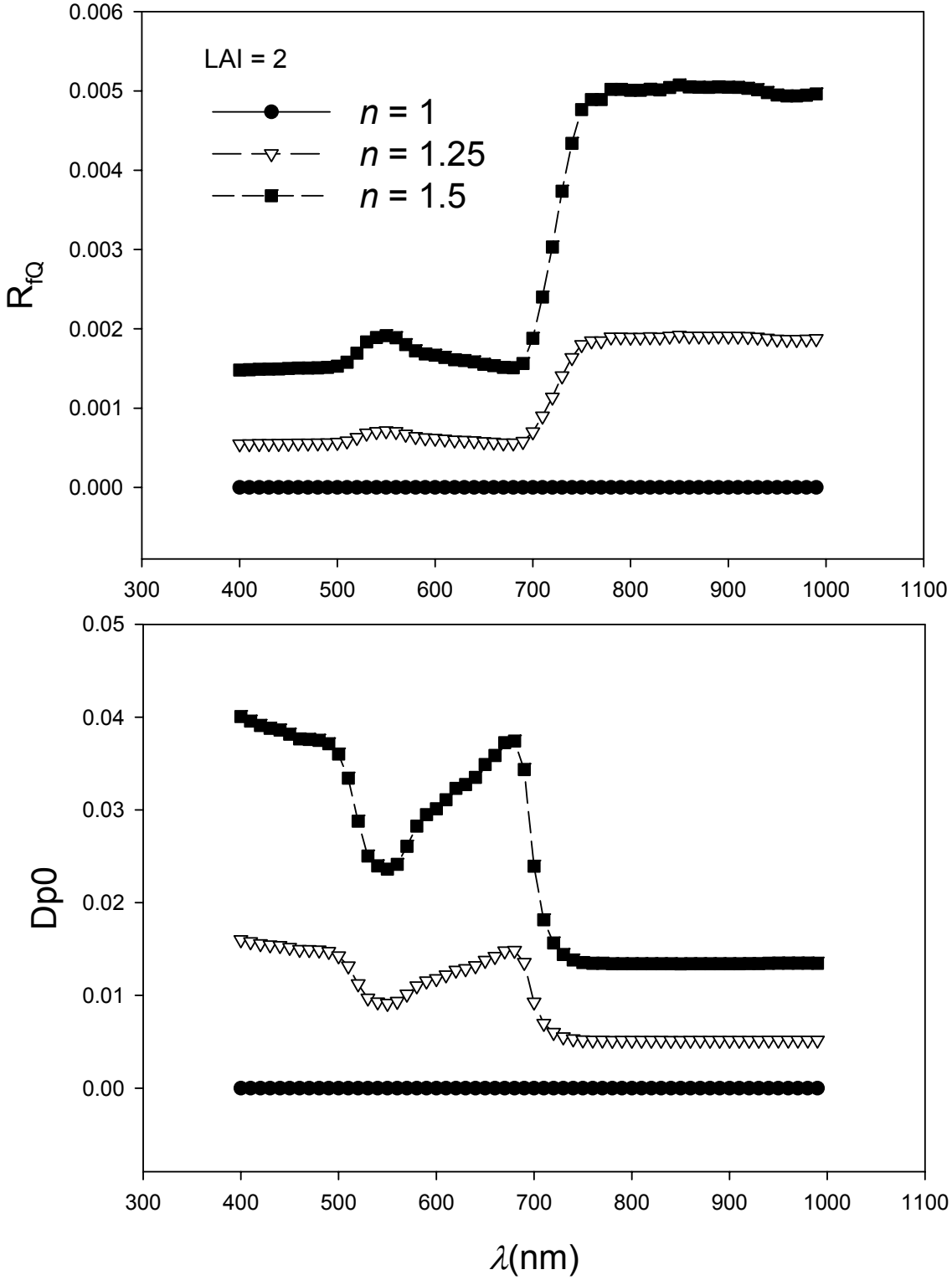

Fig. 20 Linearly polarized reflectance R_{fQ} and degree of polarization (DP0).

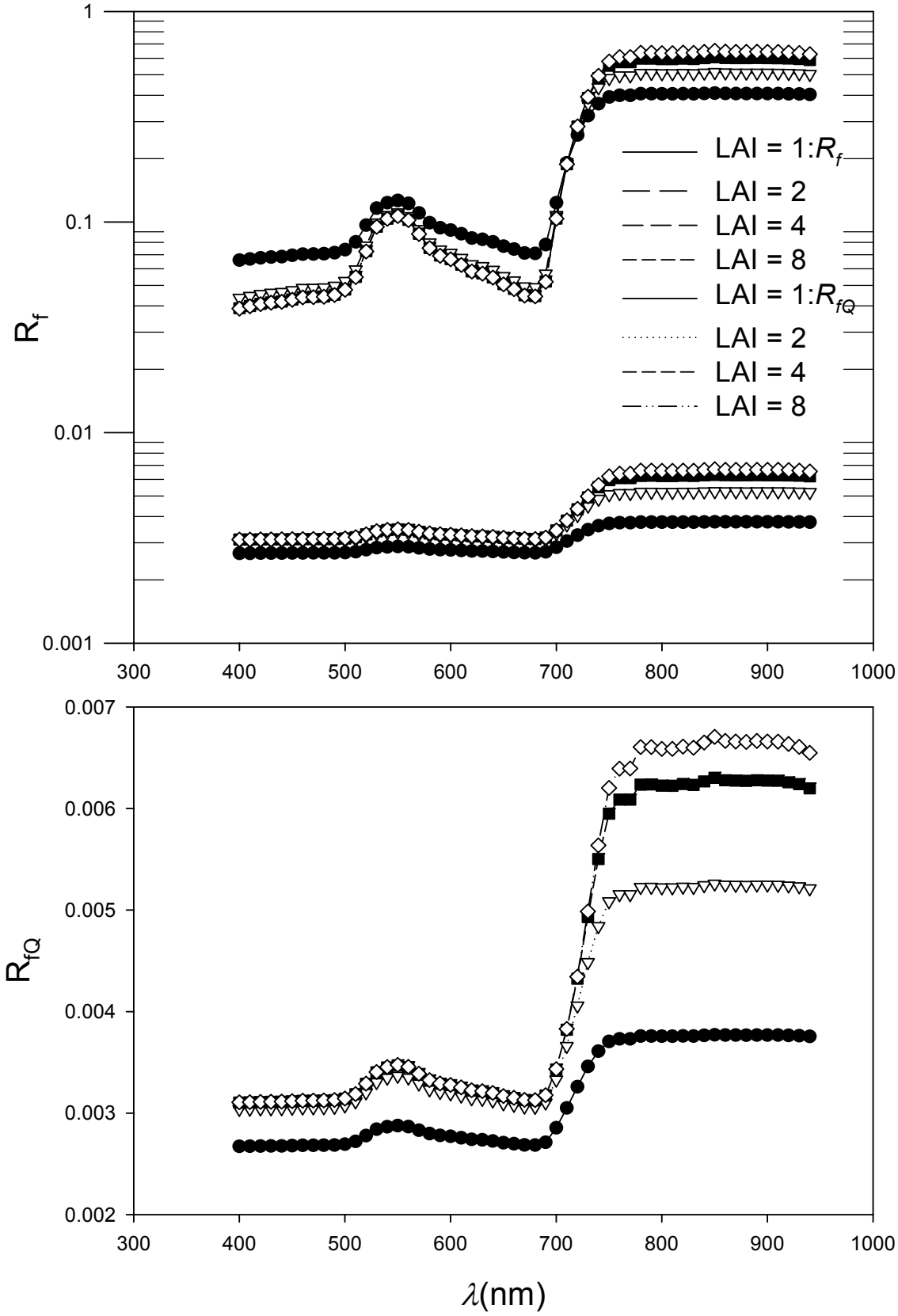

Fig. 21 Variation of LAI over unpolarized target (LAD = Planophile).

Fig. 22 Helios and Pathfinder UAVs.

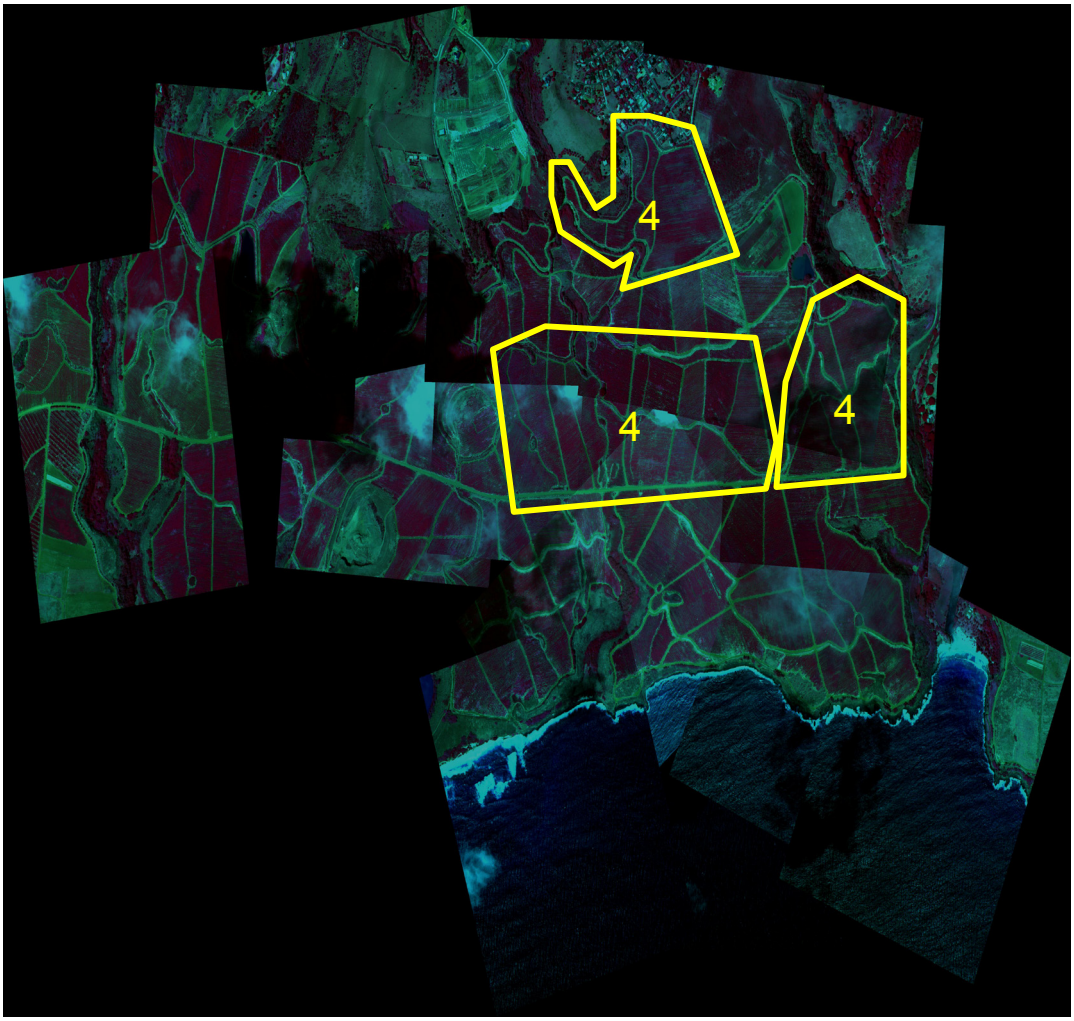

Fig. 23 Yellow coffee cherry amounts predicted in indicated fields
(Field 408 – topmost field)

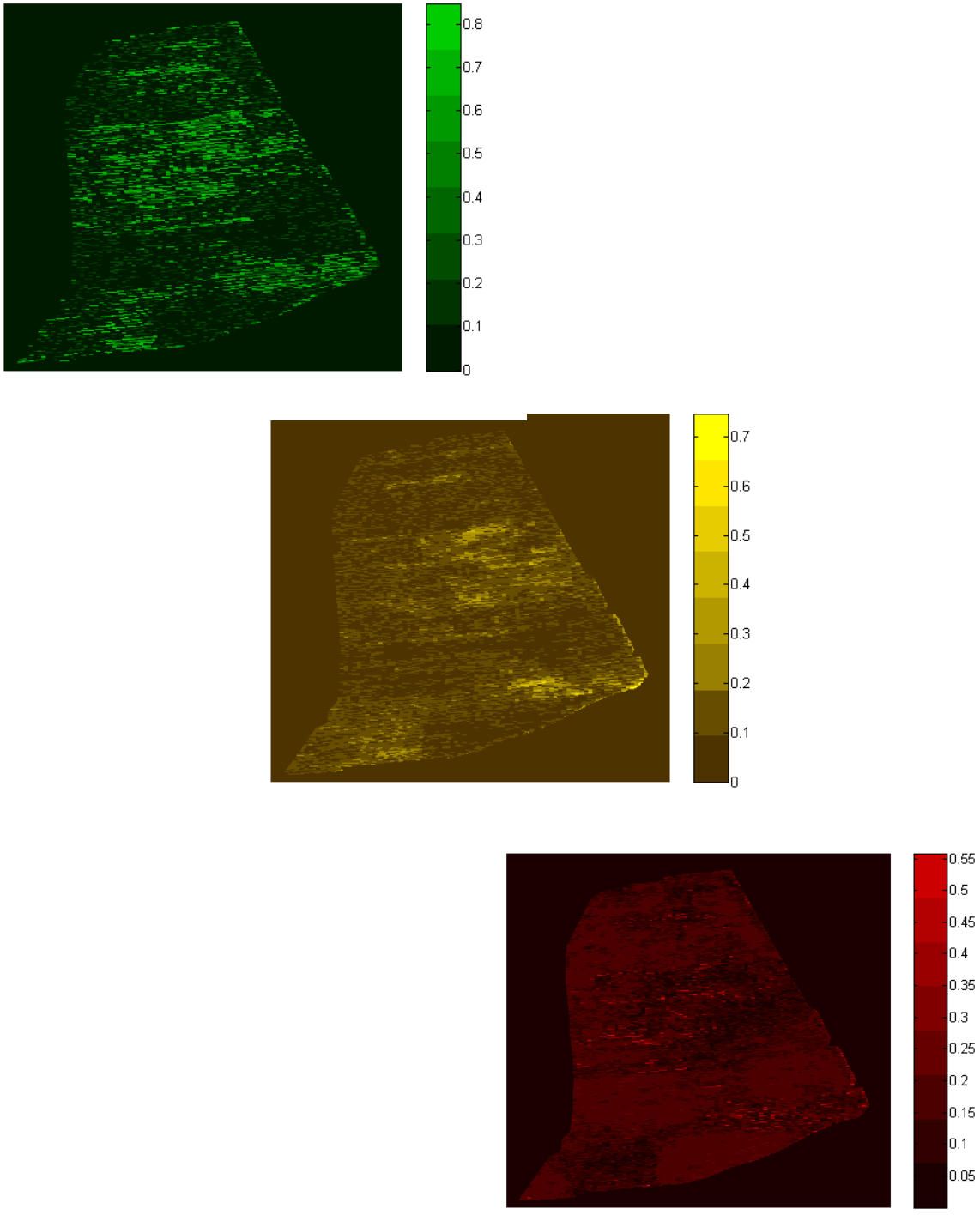

Fig. 24 Predicted green/yellow/red cherry distributions.
(Field 408 Block 4)

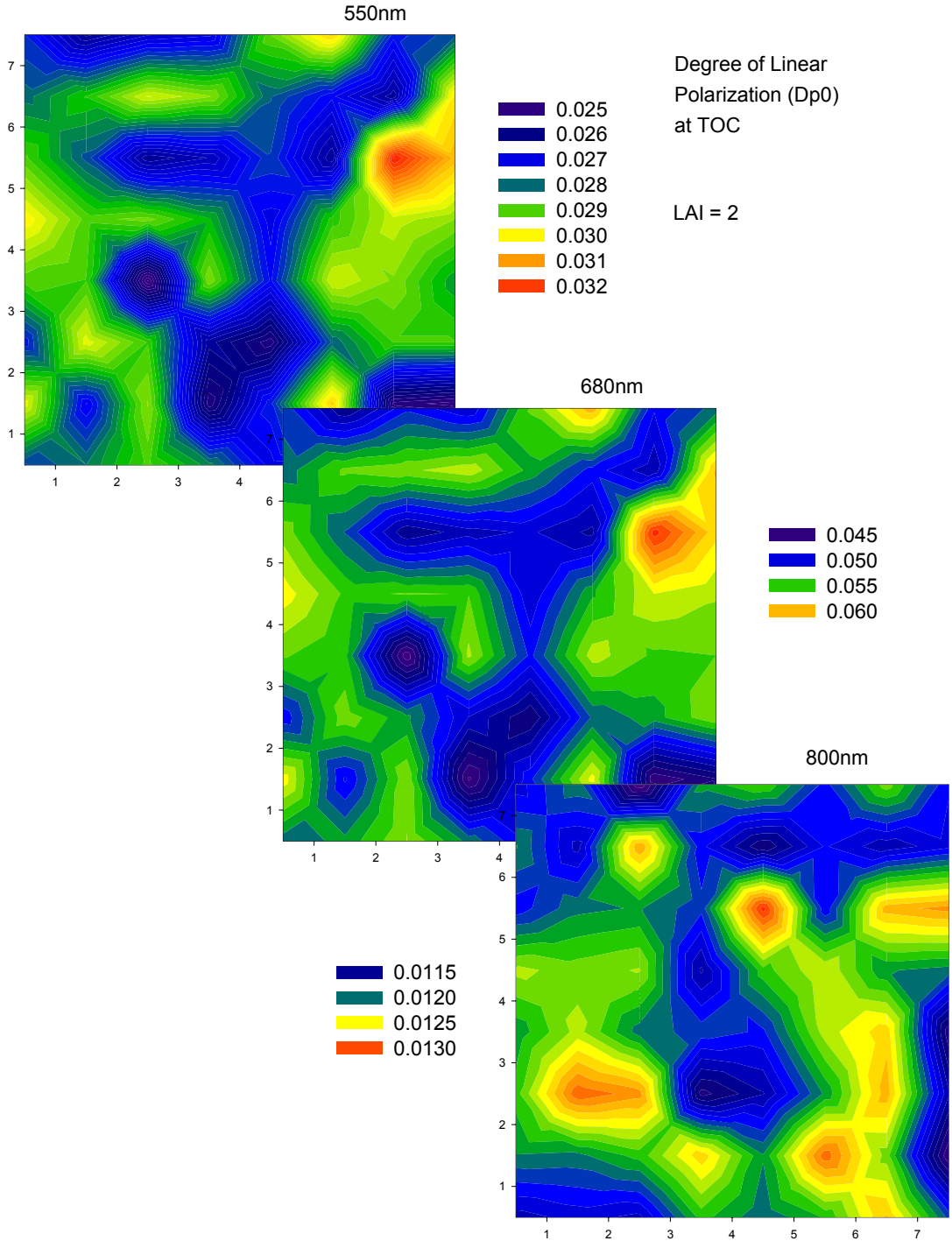

Fig. 25 Canopy reflectance for scene with a random LAD.

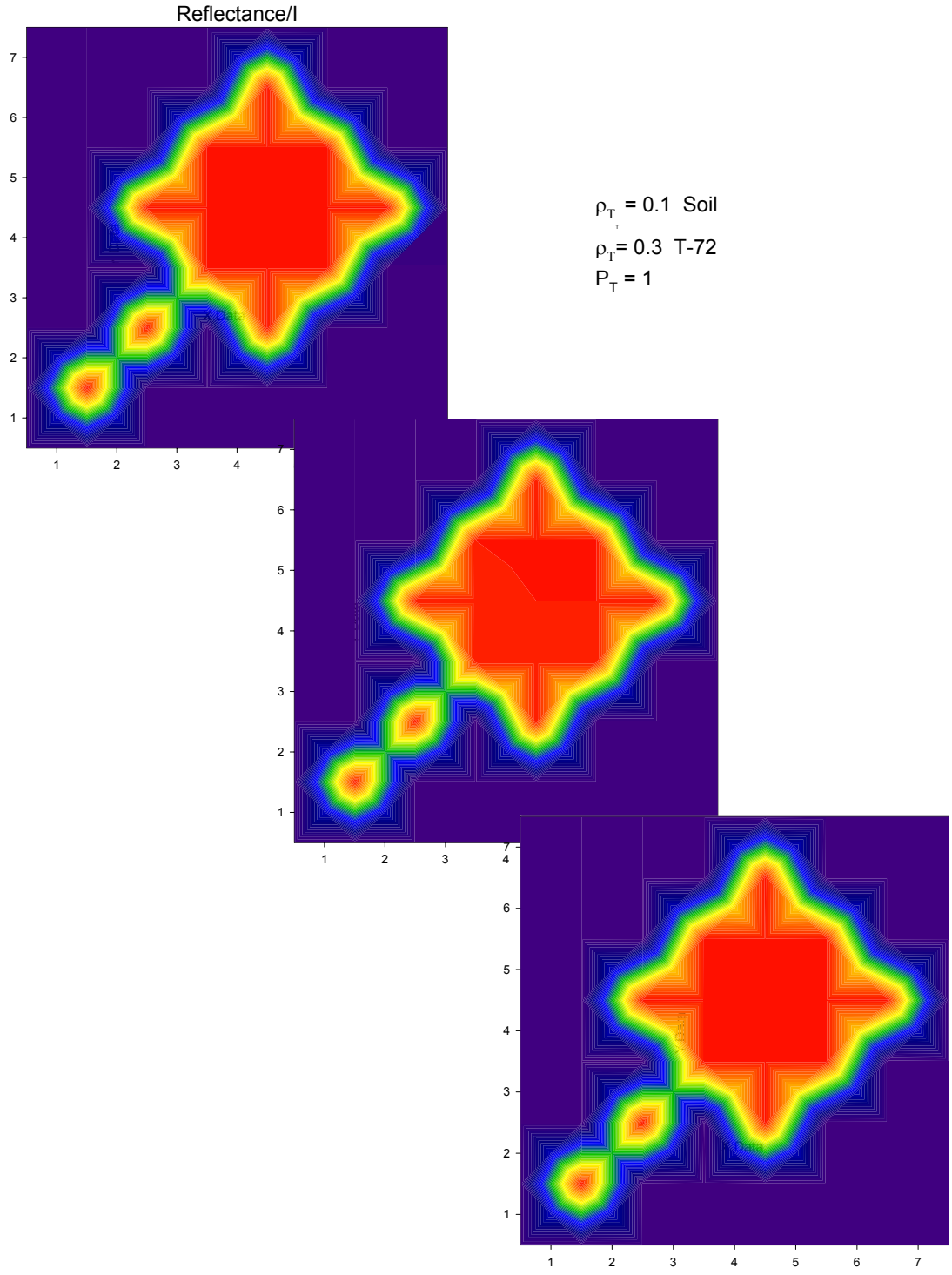

Fig. 26 T-72 tank in the clear.

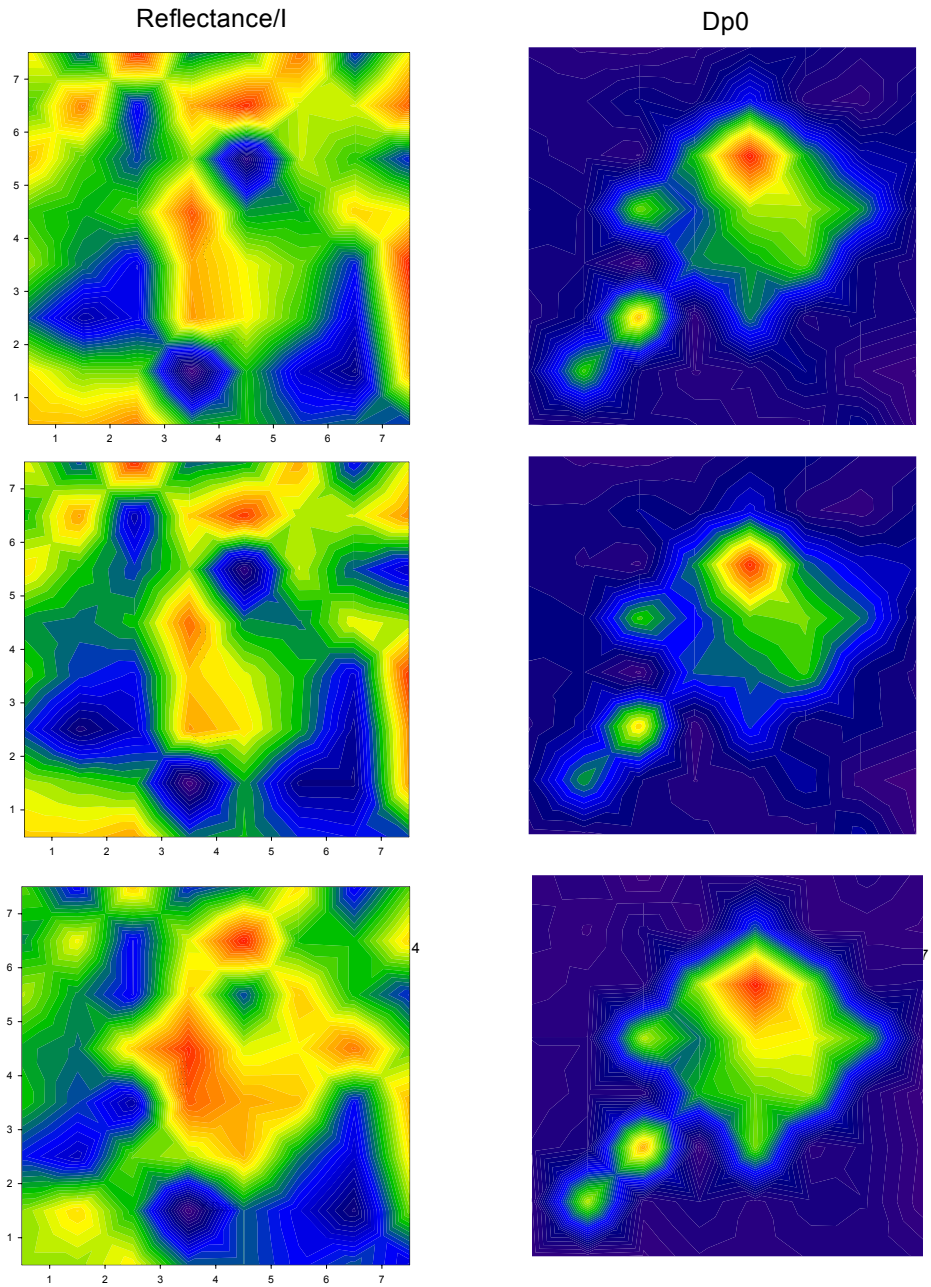

Fig. 27a T-72 under foiliage of LAI = 4.

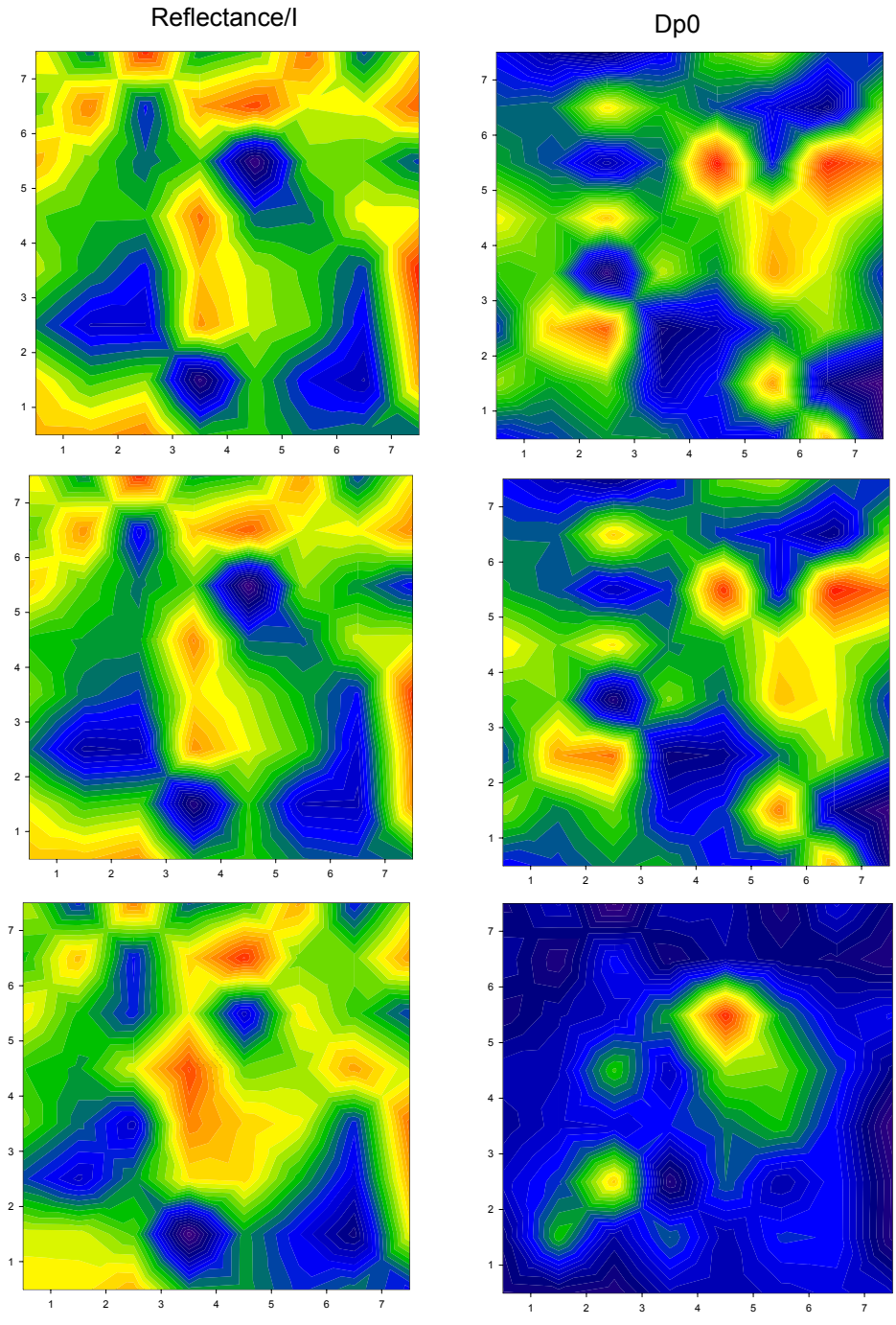

Fig. 27b T-72 under foliage of LAI = 6.

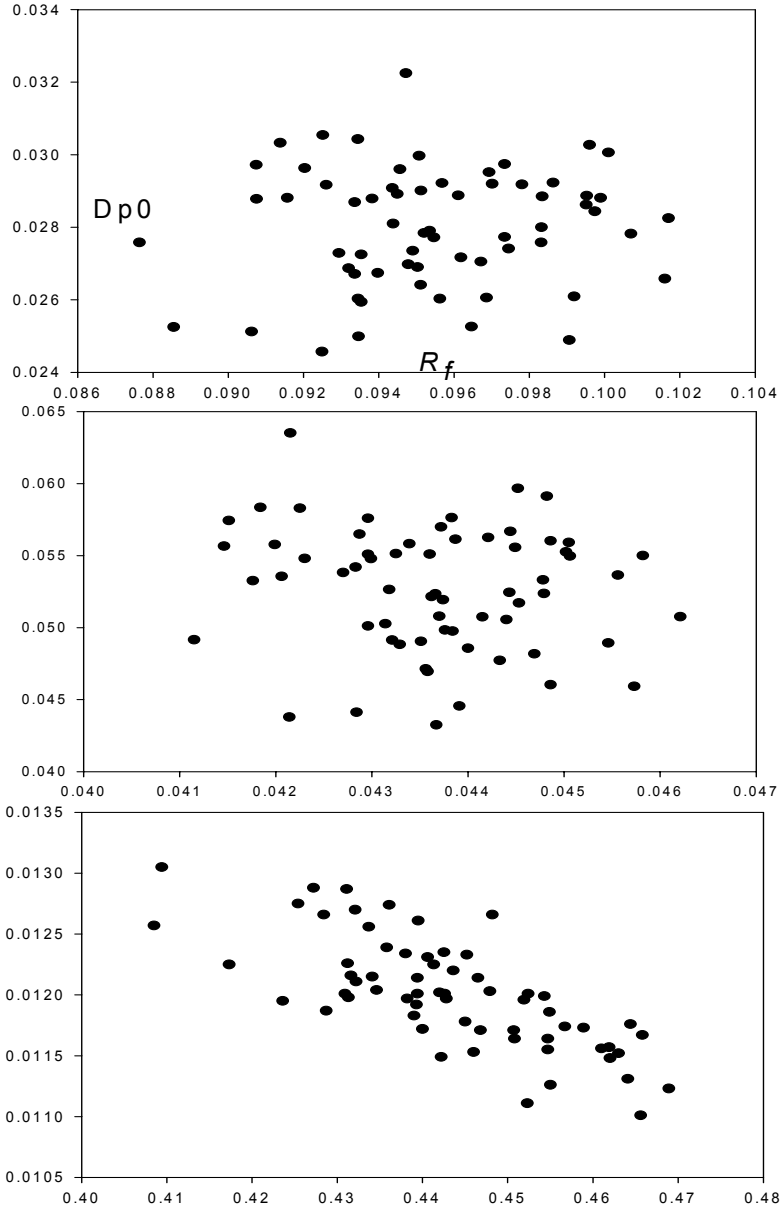

Fig. 28a Dp0 versus R_f for original scene.

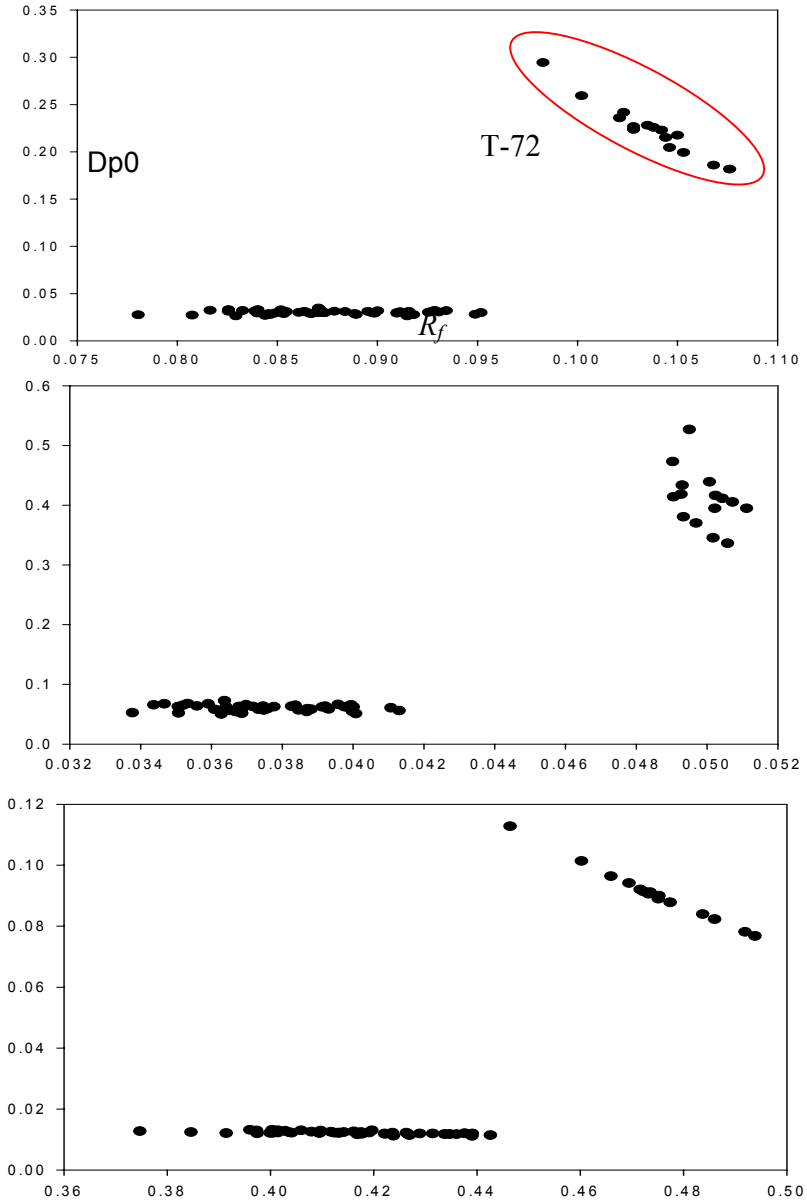

Fig. 28b Dp0 versus R_f for with T-72.